Capturing Rapid Behavioral Adaptation in an Unified Theory of the Hippocampal Cognitive Map and its Neural Implementation

Suhee Cho[1,*] **and James L. McClelland**[1,*]

[1]Stanford University, Department of Psychology, Stanford, CA 94306, USA
[*]{suheecho,jlmcc}@stanford.edu

ABSTRACT

Animals rapidly and flexibly adapt their behavior by forming an internal cognitive map. The cognitive map has been studied at multiple levels, including normative, representational, and mechanistic accounts, often focused on the role of the hippocampus. Here, we propose a framework extending the normative successor representation (SR) theory and its link to hippocampal representations and processes, incorporating recent insights into the neural basis of rapid adaptation in hippocampal areas CA3 and CA1. In our model, CA3 uses temporally symmetric behavioral time scale plasticity (BTSP) to encode spatiotemporal proximity experienced during exploration, CA1 uses temporally asymmetric BTSP to encode a perceived salience-weighted SR, and downstream areas learn successor feature predictions that can guide behavior in accordance with a behaving animal's motivational state. Through simulations of a rodent exploring a maze, we show that the network rapidly learns this representation and further strengthens the map by generating spontaneous replay activity during subsequent offline phase. Behavioral simulations show how these processes give rise to motivational state-dependent choice, rapid behavioral adaptation to changes in the availability or reward, and one-trial avoidance learning.

Introduction

Animals adapt quickly to their experience in spatial environments. This ability is closely tied to the concept of a "cognitive map"—a putative representation that receives locally available information, integrates it with internal state information, and generates signals that guide behavior[1–3]. Classic maze experiments show that rodents rapidly form the cognitive map to make efficient decisions (Fig. 1a), motivating three central questions: **(1) What is learned?** In what form is the cognitive map represented in the brain? **(2) How is it learned?** What neural mechanisms give rise to the cognitive map? **(3) How is it used?** How does the output of the cognitive map contribute to evaluating different possible choices and guiding behavior?

To address the question *What is learned?*, we build on the account of the cognitive map and its neural representation provided by the successor representation (SR)[4,5]. Rather than encoding environments purely in terms of spatial distance, the SR encodes the expected future occupancy of each location based on the animal's movement history (Fig. 1b, top). Although the SR framework is supported by several experimentally observed properties of hippocampal place cells[5], including the predictive skewing of place fields[6,7], without further elaboration it leaves many findings unaccounted for[8]. In particular, SR does not explain the stronger hippocampal encoding of behaviorally significant but infrequently visited locations, such as those associated with aversiveness[9], motivational salience[10], or novelty[11]. These factors, collectively termed perceived salience (PS)[12], provide a crucial input for rapid and flexible learning. Experimental evidence shows that hippocampal representations are modulated by PS, including increases in the number of place cells encoding salient locations[13–16] and accelerated formation of those fields[17]. Together, these findings suggest that the hippocampus integrates PS signals with spatial inputs, producing a PS-weighted SR that is more adaptive than a purely spatial SR.

To answer *How is it learned?*, we rely on behavioral time-scale synaptic plasticity (BTSP)[18], a biologically supported synaptic modification rule, to acquire a PS-weighted SR. BTSP occurs when neurons exhibit depolarization events called plateau potentials lasting hundreds of milliseconds, producing large synaptic changes linking neural activity across a time-scale of seconds, making it a promising candidate for rapid mechanism for rapid behavioral adaptation. In hippocampal area CA1, BTSP is modulated by novelty, salience, and reward[19–22], making it a compelling candidate for learning the PS-weighted SR.

Further synaptic plasticity is thought to occur when an animal is not actively exploring but is instead at rest or asleep. During this "offline" phase, hippocampal place cells are spontaneously reactivated in sequences that recapitulate trajectories through the environment[23]. This phenomenon, known as hippocampal replay, is thought to contribute to the strengthening, stabilization and/or consolidation of learning acquired during physical exploration of the environment[24–26]. Remarkably, these sequences can represent trajectories that the animal has

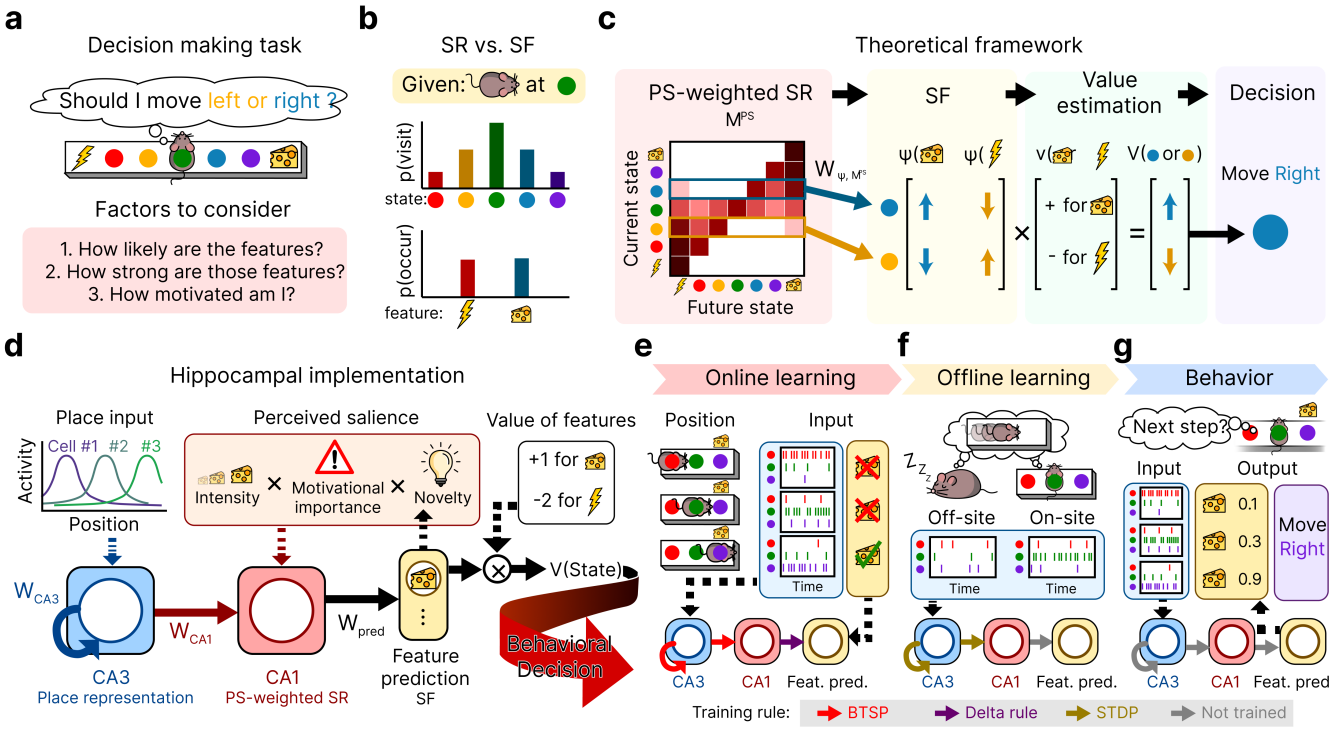

Figure 1. **a**, Rodent decision-making in a maze. **b**, Two ways of representing a state: successor representation (SR) and successor features (SF). **c**, Schematic of the theoretical framework. A PS–weighted SR is relayed to predict successor features, which are then used to compute value and guide decisions. **d**, Hippocampal implementation of the model. CA3 receives place input and encodes place representations. CA1 receives input from CA3 along with perceived salience, and encodes the PS-weighted SR. This is passed to the feature prediction layer, which encodes SFs and is ultimately used to determine the subjective value of states. **e–g**, Three distinct phases of our simulations. **e**, *Online learning*: the animal actively explores the environment and encounters features. Place input varies with position, and hippocampal weights are updated using the BTSP rule, while the feature-prediction weights are trained using an error-correcting delta rule. **f**, *Offline learning*: simulating rest or sleep. Place input is held constant, and hippocampal weights are updated using symmetric STDP while the feature-prediction weights are fixed. **g**, *Behavior simulation*: Value-based decision making in the learned track. No weights are updated. The learned connections weights are used to calculate feature predictions, which are assigned value based on current motivational state to guide behavior toward higher-valued outcomes.

never physically traversed[27], suggesting that replay helps complete the internal spatial map[28,29]. Since the plateau potentials that trigger BTSP do not occur during replay episodes[18,30], our simulations rely on a version of a spike-time dependent learning rule[31] as one possible implementation.

Finally, to answer *How is it used?*, we consider how the learned PS-weighted SR guides decisions. The original SR is limited in that it does not explain how feature-specific factors, rather than entire states, influence value[8]. For example, water becomes valuable only when the animal is thirsty, selectively increasing the value of states containing water. To address this, we incorporate successor features (SFs)[32] previously proposed in a machine learning context. Unlike the SR, which predicts the *future occupancy of states*, SFs predict *the future occurrence of features* (Fig. 1b, bottom). We propose that the PS-weighted SR is used to predict SFs in downstream brain areas. These predicted features are then assigned value based on the animal's motivational state during behavior, ultimately allowing state-specific value estimates to guide behavior.

Combining these components, we propose a unified framework of the cognitive map (Fig. 1c), its neural implementation, and its consequences for behavior. In our model, the hippocampus integrates spatial input with perceived salience signals to form a PS-weighted SR, which is then conveyed to downstream areas that compute successor features and combine them with motivational signals to estimate state values (Fig. 1d). To demonstrate how this representation emerges and supports rapid behavioral change, our simulations employ three distinct phases: an online exploration phase, during which BTSP updates hippocampal connectivity (Fig. 1e); an offline replay phase, during which spontaneous replays propagate predictive structure that is integrated into synaptic connectivity through STDP (Fig. 1f), and a behavioral phase in which the learned predictive map supports flexible value computation and guides behavior (Fig. 1g).

Results

Formal Statement of Theory, Its Neural Implementation, and Simulation Approach

Following the proposal of Dayan[4], the SR for a starting state s and a target state s' is the expected discounted future occupancy of s' across time t, given $s_0 = s$:

$$M(s,s') = \mathbb{E}\left[\sum_{t=0}^{\infty} \gamma^t \, \mathbb{I}(s_t = s') \,\middle|\, s_0 = s\right], \tag{1}$$

where $\gamma \in [0,1]$ is a discount factor. Thus $M(s,s')$ weights nearer states more heavily than distant ones.

The SR can be extended to characterize SFs, which represent predictions of future occurrence of environmental features (e.g., cues, rewards, or hazards)[32]. Let $\phi(s',f)$ denote the expected presence of feature f at state s'. The SF for feature f at start state s is defined as the expected discounted future occurrence of that feature:

$$\begin{aligned}\psi(s,f) &= \mathbb{E}\left[\sum_{t=0}^{\infty}\gamma^t\,\phi(s_t,f)\,\middle|\,s_0=s\right] \\ &= \sum_{s'} M(s,s')\,\phi(s',f).\end{aligned} \tag{2}$$

We further incorporate perceptual salience (PS), $\omega(s')$ into our framework[8,12]. First, we define the PS-weighted SR,

$$M^{\mathrm{PS}}(s,s') = \omega(s')\,M(s,s'). \tag{3}$$

That is, PS amplifies states by $\omega(s')$ in the SR. With this scaling, the SF can be expressed as a linear map from M^{PS}:

$$\psi(s,f) = \sum_{s'} M^{\mathrm{PS}}(s,s')\cdot W_{\psi,M^{\mathrm{PS}}}(s',f), \qquad \text{where} \tag{4}$$

$$W_{\psi,M^{\mathrm{PS}}}(s',f) = \frac{\phi(s',f)}{\omega(s')}. \tag{5}$$

Finally, the value of state s is defined as the sum of successor features weighted by their value:

$$V(s) = \sum_{f}\psi(s,f)\,v(f), \tag{6}$$

where $v(f)$ is the value of feature f at the time when $V(s)$ is estimated. This allows the same predictive representation ψ to flexibly support different decisions, depending on the agent's internal motivational state.

We link these theoretical quantities to neural processes and behavior as follows:

- An estimate of the **PS-weighted SR**, $M^{\mathrm{PS}}(s,s')$, is acquired through BTSP in hippocampal areas CA3 and CA1 during exploration and is further reinforced through replay-driven plasticity.
- **Perceived salience**, $\omega(s)$, is determined based on the intensity, novelty, and motivational significance of features present at state s is incorporated to the CA1 representation by modulating BTSP.
- The **mapping from PS-weighted SR to SF**, $W_{\psi,M^{\mathrm{PS}}}$, is instantiated by learned synaptic weights from the CA1 area to downstream feature-encoding populations.
- **State value**, $V(s)$, is computed in extra-hippocampal circuits integrating feature predictions with feature-specific value signals $v(f)$, which depend on the animal's internal needs during behavior.
- The resulting $V(s)$ guides **decision making**: when selecting actions, animals preferentially transition to states with higher $V(s)$.

In the following sections, we modeled neural activity and behavior after simulated exposure to environments paralleling those used in published experiments. See *Methods* for details of the distinct simulation paradigms used for the online exploration, offline replay, and behavior phases of these simulations (Fig. 1e–g).

Representations in CA3 and CA1 regions emerge rapidly through BTSP, supporting replay and prediction of successor features

Extending prior work[30,33], we developed our own simplified implementation of BTSP-driven learning in hippocampal areas CA3 and CA1, and added circuitry to learn SF representations. The model includes a CA3-like neural population with recurrent weights W_{CA3} and a CA1-like population with feedforward weights W_{CA1} from CA3 to CA1. For simplicity, each CA3 neuron receives place-specific input in the form of a prespecified Gaussian bump, with the centers of the bumps evenly covering a simulated linear track. On the other hand, CA1 neurons only received input via W_{CA1} from CA3. We added a downstream "feature-prediction" population of neuron-like units, each of which was assigned to correspond to a specific environmental feature, with weights W_{FP} projecting to it from CA1. We divided the linear treadmill into eight consecutive states (states 1–8), each of which was associated with a unique neutral "background" feature to distinguish spatial locations (Fig. 2a).

We modeled BTSP-driven online learning through 5 contiguous laps of navigation— uniform movement through the assigned CA3 place field centers. During the online learning, W_{CA3} was trained using the BTSP learning rule with a symmetric time kernel, whereas W_{CA1} was trained using an asymmetric kernel (Fig. 2b), reflecting experimental findings[18,21,30]. W_{FP} was trained using an error correcting delta rule[34] to predict the presence of the eight background features associated with the track states (Fig. 2l).

We first examined the learning of W_{CA3} and W_{CA1}. As expected, the distinction in learning kernels resulted in different structures in these connections. To illustrate this, we separately identified CA3 and CA1 neurons by rank-ordering them according to the position at which each neuron exhibited its peak firing rate, from left to right along the track. Then, we plotted W_{CA3} and W_{CA1} after lap 5, arranging both pre-synaptic and post synaptic neurons by their IDs (Fig. 2c). The results showed that W_{CA3} encoded spatial relationships between place fields in an allocentric-, movement direction-independent manner, resulting in a symmetric structure (Fig. 2d, blue). In contrast, W_{CA1} displayed a skewed distribution: connections from place cells representing positions behind the animal's current location were more potentiated than those ahead (Fig. 2d, red).

Next, we examined the functional consequences that ensued from these distinct representations. We first showed that

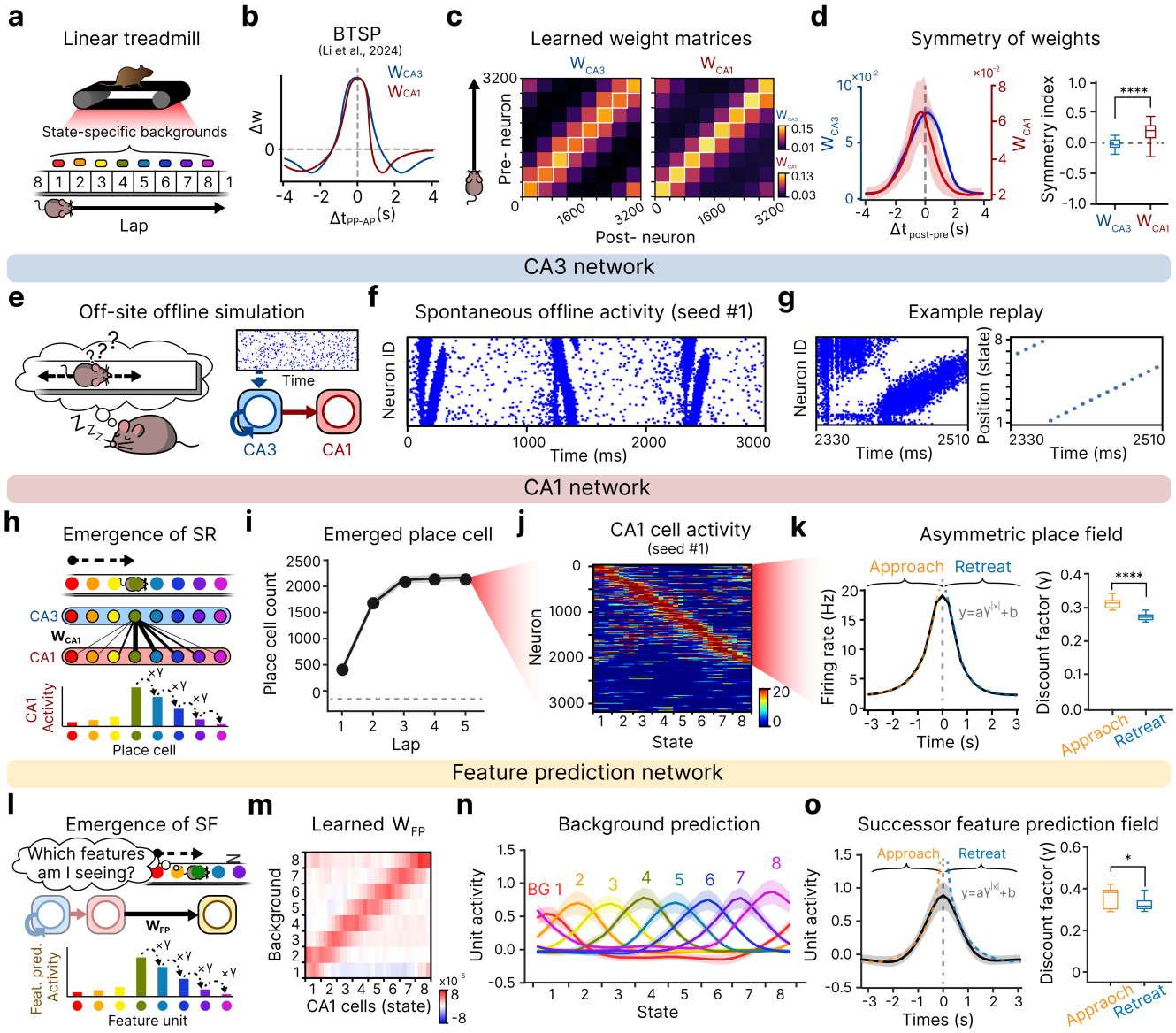

Figure 2. **a**, Linear treadmill simulation setup. **b**, BTSP weight update kernels for CA3 and CA1. **c**, Weight matrices after lap 5 with place cells sorted by field location, binned into 8 groups and averaged. Left: W_{CA3}. Right: W_{CA1}. **d**, Left: Averaged synaptic weights of postsynaptic neurons aligned by presynaptic index, for W_{CA3} (blue) and W_{CA1} (red). The curve is divided into weights from presynaptic neurons with smaller indices ("behind") and larger indices ("ahead"). Right: Symmetry index of W_{CA3} and W_{CA1}, calculated by normalizing the area of behind vs. ahead weights. Paired t-test, $N_{seed} = 10$, $^{****}P = 4.58 \times 10^{-36}$. **e–g**, Results from CA3. **e**, Offline simulation schematic. **f**, Example spontaneously generated offline activity. **g**, Left: Example replay activity. Right: Decoded position. **h–k**, Results from CA1. **h**, SR emerges in CA1 due to asymmetry of W_{CA1}. **i**, Number of CA1 place cells formed after each lap. **j**, CA1 place fields after lap 5. **k**, Left: Average firing rate across place fields. Right: Fitted discount factors for approach vs. retreat trajectories relative to field centers. Paired t-test, $N_{seed} = 10$, $^{****}P = 7.02 \times 10^{-5}$. **l–o**, Results from the feature prediction layer. **l**, Learning W_{FP} to predict SFs. **m**, W_{FP} after lap 5. **n**, Predictions for each background feature across positions after lap 5. **o**, Average predicted presence for the current state vs. non-current states. Paired t-test, $N_{seed} = 10$, $^{***}P = 8.13 \times 10^{-4}$. All data are presented as mean±s.d.

online learning through the symmetric BTSP rule enabled the CA3 network to spontaneously generate replay-like activity during the following offline periods. To test this, we simulated the offline phase by delivering a uniform, non-spatial input for three seconds to the trained W_{CA3} (Fig. 2e). We simulated the resulting spontaneous activity using biophysically plausible parameters and an adaptive exponential intergrate-and-fire neuron model (Supplementary Materials, Section 3)[31].

The result demonstrated that CA3 neurons fired in sequence according to their place-field locations (Fig. 2f). These sequential events were best decoded as a linear travel along the track and therefore qualify as replay events[35] (Fig. 2g). The replay activity began to emerge after a single track traversal and was robust after 5 laps of exploration (few-shot learning)[36]. In contrast, networks trained with STDP during exploration as in prior work[31] required approximately 400 laps before exhibiting comparable replay dynamics (Supplementary Fig. 2).

Next, we showed that the asymmetric structure of W_{CA1} endows CA1 neurons with SR-like place fields (Fig. 2h) after 5 laps of learning from random initial weights. We classified a CA1 neuron as a place cell if its peak firing rate exceeded 15 Hz (75% of the model's specified maximum of 20 Hz) at any position along the track (see *Methods* section for details). We found that an average of 2,148 CA1 place cells had emerged (Fig. 2i). The resulting place fields were distributed across the environment (Fig. 2j, Supplementary Fig. **??**). As expected, these place fields were asymmetric: neurons began firing earlier as the animal approached the field's peak location and shut off more rapidly as it moved away (Fig. 2k, left). This was assessed by modeling the place cell activity during the "approach" and "retreat" from the center of the receptive field using the function $y = a \times \gamma^{|x|} + b$ (Fig. 2k, right), where the larger discount factor γ during approach compared to retreat reflects the expected asymmetry.

Finally, we demonstrated that the feature prediction network successfully learned to anticipate environmental features (Fig. 2l). As expected, by the end of the fifth lap, W_{FP} had become state-specific, with CA1 place cells preferentially projecting to the feature unit associated with their place field (Fig. 2m). Consequently, each background feature unit exhibited strongest prediction when the animal occupied its corresponding location (Fig. 2n), along with the anticipatory activation similar to that seen in the CA1 place fields (Fig. 2o).

Salient features are rapidly encoded and updated in CA1 and in the feature prediction network

Next, we demonstrated that the SR encoded within the CA1 layer reflects the introduction and relocation of salient outcomes[18,22], leading to rapid adaptation of place fields and outcome predictions. We introduced a food reward as a salient outcome after simulating five familiarization laps without food reward (Figure 2). The food was placed at state 4 for next five laps (laps 6-10), and then relocated to state 8 for five additional laps (laps 11-15) (Fig. 3a). We treated the introduction of reward as affecting two key factors (Fig. 3b). First, the motivational importance of food was set to 3, compared with 1 for background states. This significantly increased the perceived salience of the reward location, modulating the place field formation in CA1. (Fig. 3c). Second, the animal's travel speed was halved when passing through the reward state reflecting slowing during reward consumption[18,22].

We next examined whether the SR encoded within W_{CA1} captured the salience information introduced by the reward. As expected, W_{CA1} adapted rapidly to changes in reward location, while W_{CA3} was not meaningfully altered (Fig. 3d and e). After initial reward introduction, a part of W_{CA1} representing state 4 were selectively strengthened. Following reward relocation, W_{CA1} projecting from neurons representing the new reward location (state 8) increased sharply. This adaptive reweighting arises from the adaptive nature of BTSP in CA1, which modulates synaptic strength according to perceived salience (Supplementary Fig. 3). As a result, the CA1 neurons were adaptively remapped to over-represent the vicinity of the reward (Fig. 3f and g)[13,14,21].

We next examined how these representational changes improved reward prediction, distinguishing between novel conditions (immediately following reward introduction or relocation; Fig. 3h, left) and familiar conditions (after repeated exposure; Fig. 3h, right). As CA1 reorganized to over-represent the reward location (Fig. 3g), CA1 population activity at that state increased rapidly following a novel reward encounter (Fig. 3i). This increase was larger and faster than the population-level changes induced by learning background features. Elevated CA1 population activity, in turn, accelerated learning of the reward–state association: prediction error for the reward decreased much more rapidly than for background features (Fig. 3j).

In contrast to these rapid cell-level changes, behavioral adaptation showed more gradual development. Immediately after the reward was introduced at state 4, the network started to predict the reward at the reward location and to anticipate it at the preceding state, demonstrating one-shot learning (Novel; Fig. 3k). This prediction was gradually strengthened With repeated exposure to the reward at the same location (Familiar; Fig. 3k). After reward relocation to state 8, CA1 partially retained residual over-representation at the former reward site. Nevertheless, the feature-prediction layer rapidly shifted to predict reward at the new location (Novel; Fig. 3l), while prediction at the old site decayed gradually with further experience (Familiar; Fig. 3l). This asymmetric adaptation reflects rapid acquisition of new salient associations alongside slower decay of memories about the previous location[9,37].

Learning to seek rewards relevant to current motivational state

We next explored how our framework supports using learned feature predictions to obtain rewards, highlighting use of these predictions to seek rewards relevant to an animal's motivational state at the time when it is behaving. Using a setup

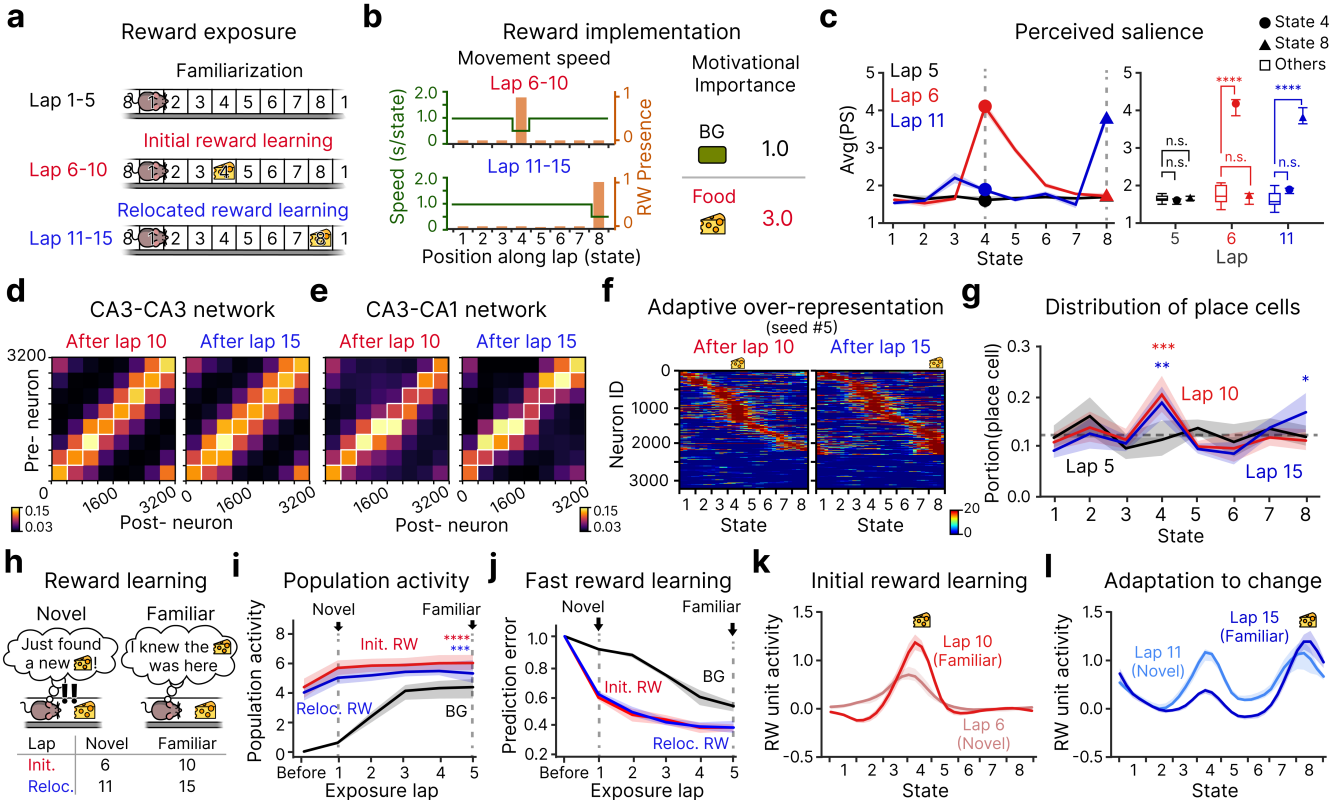

Figure 3. **a**, Simulation scheme for introducing a salient reward. **b**, Two factors modulated by reward introduction: reduced movement speed and increased motivational importance. **c**, Left: Average perceived salience across states during laps 5, 6, and 11. The rewarded state exhibits elevated perceived salience when the reward is present. Right: Perceived salience at states 4, 5, and all other states during laps 5, 6, and 11. Paired t-test, $N_{\text{seed}} = 10$, n.s. $P > 0.05$, $^{***}P < 0.005$. **d**, W_{CA3} after lap 10 (initial reward introduction) and lap 15 (reward relocation). Values are averaged across 10 random seeds. **e**, W_{CA1} after lap 10 and lap 15, averaged across 10 random seeds. **f**, CA1 place cell activity after lap 10 and lap 15. Place fields cluster around reward locations and adapt following reward introduction and relocation. **g**, Proportion of CA1 place cells representing each state after lap 5, lap 10, and lap 15. The dashed line indicates the expected proportion (1/8) for a uniform distribution. One-sample one-tailed t-tests comparing mean $< 1/8$, $N_{\text{seed}} = 10$; $^{*}P < 0.05$, $^{**}P < 0.01$, $^{***}P < 0.005$; unmarked comparisons are not significant with $P > 0.05$. **h**, Two cognitive states associated with reward perception. A reward is initially experienced as novel (left) and becomes familiar after repeated exposures at the same location (right). **i**, Development of CA1 population activity at reward-related states as the animal becomes familiar with environmental features. Population activity was computed as the mean firing rate across all CA1 neurons. The black line shows activity at state 4 from the initial network through lap 5, the red line shows activity at state 4 from lap 5 to lap 10 (reward present), and the blue line shows activity at state 8 from lap 10 to lap 15 (after reward relocation). Paired t-test, $N_{\text{seed}} = 10$, ****: CA1 population activity at state 4 at at lap 10 vs. CA1 population activity at lap 5, $P = 5.70 \times 10^{-7}$, ***: CA1 population activity at state 8 at at lap 15 vs. CA1 population activity at lap 5, $P = 0.004$. **j**, Prediction error for background features and the reward feature across laps. Background features require more laps to learn than the reward feature. **k**, Reward learning following initial introduction at state 4. **l**, Reward learning following relocation to state 8. All data are presented as mean $\pm$ s.d.

similar to one used in an experiment demonstrating state-dependent reward seeking[10], we trained the network on a two-dimensional T-maze with two distinct arms. During the exploration phase, we simulated alternating visits to each arm: In every odd lap, the animal started at the stem (state 1) and moved toward the left arm (state 4), whereas in every even lap it moved toward the right arm (state 10) (Fig. 4a). After six laps (three exposures to each arm), two distinct reward features were introduced at the arm ends (food and water) and the animal was exposed to each reward twice (laps 7–10) (Fig. 4b).

After lap 10, W_{CA3} encoded the structural layout of the T-maze, while W_{CA1} over-represented both arms, reflecting the presence of food and water (Fig. 4c). Correspondingly, the feature prediction layer strongly predicted each reward at its respective location (Fig. 4d).

We then simulated a behavior based on the resulting learned map under different motivational needs for food and water (Fig. 4e). In each simulation, the animal started at the stem (state 1) and and updated its location across a series of steps at a notional rate of once per second. At each step, it evaluated neighboring states and the current state, and translated these values into movement probabilities (Fig. 4f, also see Methods). Each behavioral trial lasted up to 60 seconds; if neither goal was reached, the trial ended.

We simulated three motivational conditions: (1) hungry (food need = 5, water need = 1), (2) thirsty (food need = 1, water need = 5), and (3) neutral (food need = 1, water need = 1). For each condition, we computed the Markov transition matrix containing the movement probabilities (Fig. 4g). The three matrices notably differed in the state transition probabilities from state 7 (row index highlighted in red) which is the choice point in the maze. When hungry, the animal was more likely to move toward the food arm (left), whereas

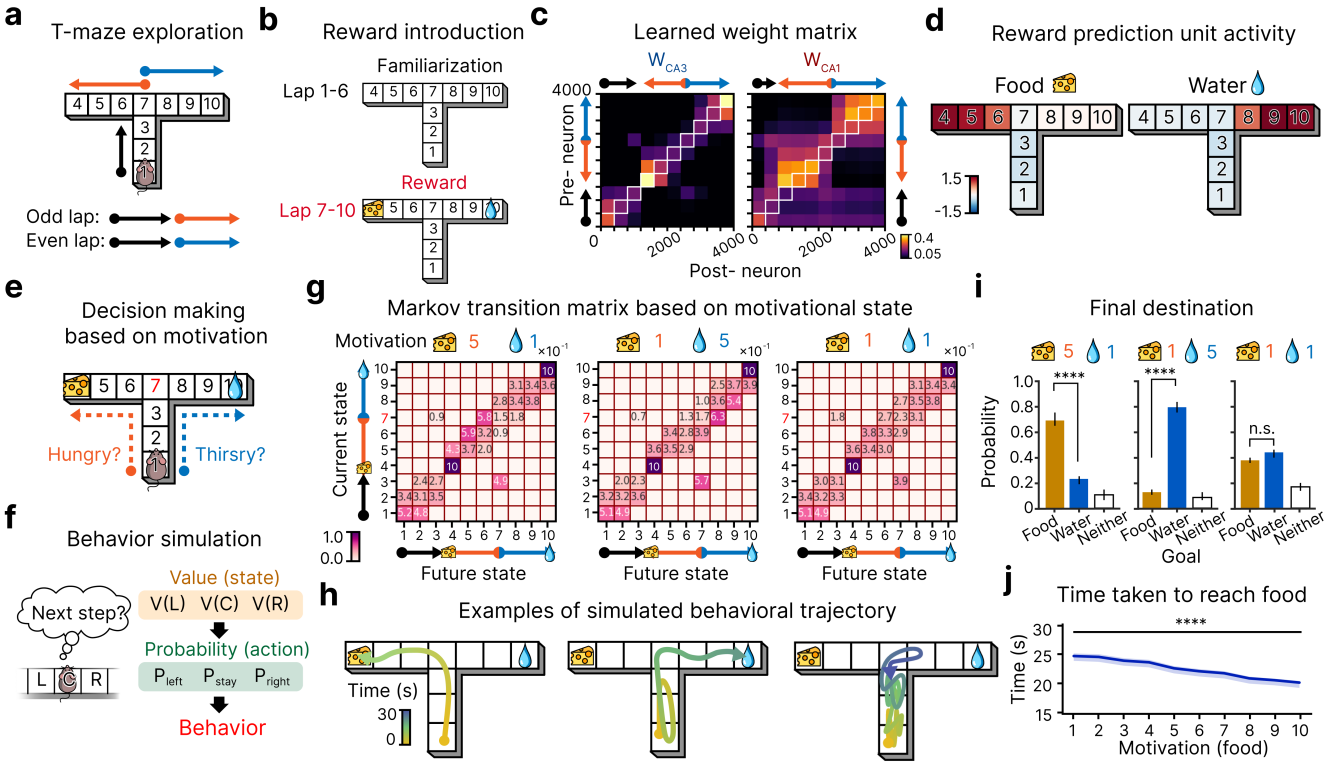

Figure 4. **a**, T-maze learning scheme. **b**, After 6 familiarization laps, two distinct rewards (food and water) are introduced at each arm for 4 laps. **c**, Resulting W_{CA3} and W_{CA1} after lap 10. **d**, Predictions for food and water across maze positions. **e**, Animal's decision to pursue either arm of the maze based on its motivational state. **f**, Behavioral decision-making simulation scheme. The choice-making point (state 7) is marked red. **g**, Markov state transition matrices under three different motivational scenarios for food and water. Transition probabilities at state 7 shows most prominently the role of motivational state and therefore marked red. **h**, Example simulated trajectories for each scenario. **i**, Goal reached within 50 seconds of movement for each scenario. Paired t-test, $N_{seed} = 10$, ****$P < 0.0005$, n.s. $P = 0.98$. Data are presented as mean±s.d. **j**, Time to reach the goal as a function of motivational strength. Mann-Kendall test, $N_{seed} = 10$, ****$P = 8.30 \times 10^{-5}$, $Z = -3.94$. Data are presented as mean±s.e.m.

when thirsty it preferred the water arm (right). Under neutral conditions, movements left, right, or back to the stem were roughly balanced. Accordingly, the animal predominantly reached the food when hungry, the water when thirsty, and distributed its choices more evenly under neutral conditions (Fig. 4h-i). Finally, we found that stronger motivational drives accelerated goal-directed behavior: as the motivational need for food increased from 1 to 10 (with water fixed at 1), the time required to reach the food decreased (Fig. 4j).

Offline replay propagates salience information to unexperienced paths, enhancing reward seeking from novel starting locations

We next investigated how learning during offline replay episodes can enhance the network's prediction of salient outcomes and support behavior, including finding novel paths to reward, as observed in the seminal experiments of Tolman[1]. We used network weights learned through BTSP after exposure to food and water reward as described above (Fig.[?]). Specifically, we hypothesized that replay activity propagates SF information across the maze, including to positions that were never visited in succession during online exploration[27] (Fig. 5a). Accordingly, we simulated an offline phase corresponding to a post-reward pause at the food location by providing place input for state 4 to CA3 cells, then observed the resulting spontaneous network activity. During this offline phase, replay activity of place cells spontaneously emerged (Fig. 5b, top).

Strikingly, the replay events we observed propagated not only along previously experienced trajectories (left- and right-arm replays), but also exhibited a novel "shortcut replay" connecting the two arms that had never been physically traversed in sequence (Fig. 5b).

We then examined how each replay type can contribute to propagating feature predictive information from the reward location to distant states. During replay, we used a temporally symmetric-spike-time dependent learning rule[31] that adjusts synaptic weights after every spike with smaller magnitude and a narrower temporal window than BTSP (Fig. 5c).

To identify distinct effects carried by different types of replay events, we determined the change in food prediction unit activity at each state, averaged over all replays of the same type that were observed during the 5-second replay period. Following shortcut replay events, food prediction increased across both arms of the maze. In particular, this update was most prominent at states proximal to the food location (states 4-7; Fig. 5d, left). Similarly, left-arm replay enhanced food prediction along the replayed trajectory (Fig. 5d, middle). In

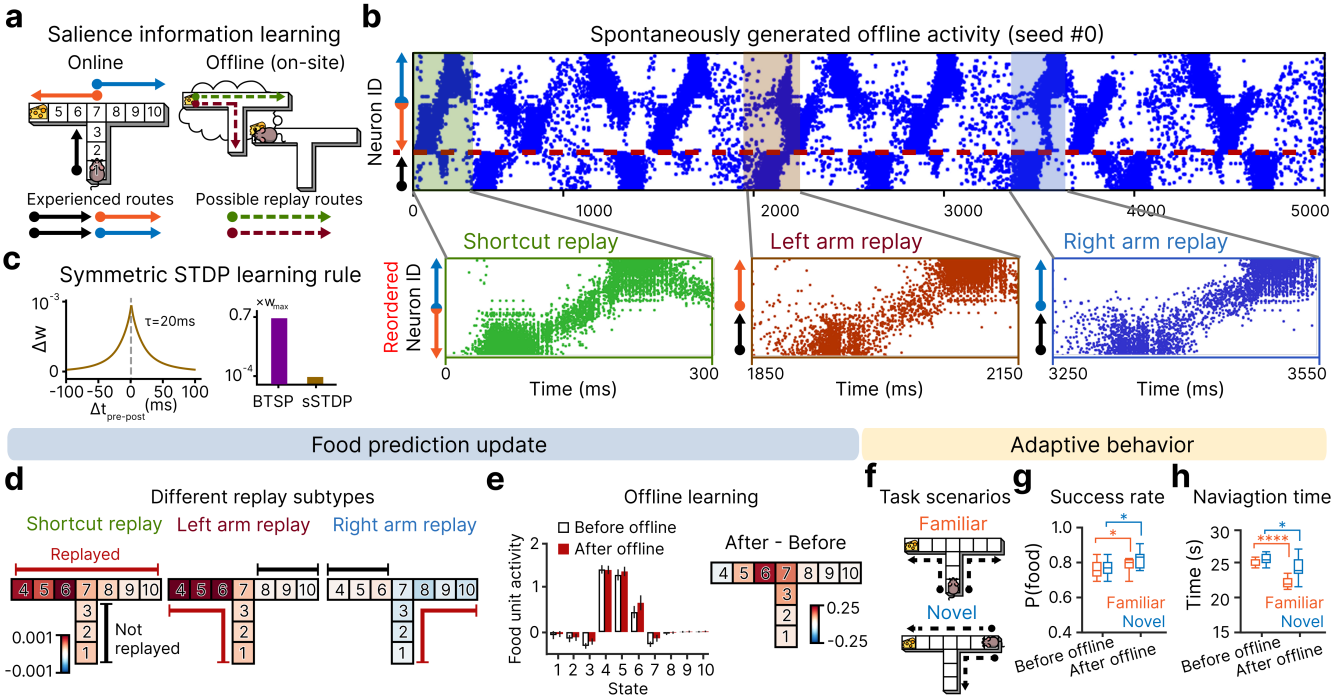

Figure 5. **a**, Propagation of salience information through online and offline learning. **b**, Spontaneously generated offline activity. Replay events are grouped into three categories based on their trajectories: shortcut, left-arm, and right-arm. For visualization, each expanded example shows only the neurons participating in the corresponding replay, reordered in the sequence in which they were activated along the replay trajectory. **c**, Left: sSTDP rule used in offline learning. Right: Largest possible weight update of BTSP and sSTDP rules. **d**, State-wise food prediction updates induced by a single replay event, shown separately for each replay subtype. Updates were computed as the difference between post-replay and pre-replay food predictions. **e**, State-wise food prediction updates induced by 5 seconds of offline learning. Left: Food unit activity at each state before (pre) and after (post) offline learning. Right: State-wise prediction updates computed as the difference between post- and pre-offline learning activity. **f**, Two behavioral simulation schemes. Left: Simulation starting from the same start position as during online exploration. Right: Simulation starting from a different start position. Both tasks aim to find food located at the same position as in the online exploration. **g**, Proportion of trials in which the animal reached the goal location within 50 seconds in familiar and novel scenarios, without and with offline learning. Paired t-test, $N_{seed} = 10$, Familiar $^*P = 0.03$; Novel $^*P = 0.02$. **h**, Time taken for the animal to reach the goal location in familiar and novel scenarios, without and with offline learning. Paired t-test, $N_{seed} = 10$, Familiar $^{****}P = 1.15 \times 10^{-5}$; Novel $^*P = 0.04$. All data are presented as mean±s.d.

contrast, right-arm replay had minimal impact, as its trajectory does not include the food location and therefore does not directly strengthen synapses originating from food-related place cells (Fig. 5d, right). Finally, we updated W_{CA1} using the full spike trains recorded during the offline simulation containing multiple replay events of different subtypes. This offline update selectively increased food prediction in reward-adjacent states, particularly those that had not strongly predicted food prior to replay (Fig. 5e).

We then simulated two behavioral task scenarios. In the first scenario, the animal started at the stem (state 1) with a motivational need of 5 (Fig. 5f, top), as during the online exploration phase (Fig. 4). Each trial ended when the animal reached either end of the maze (state 4 or state 10) or failed to reach a goal within 50 steps. In the second scenario, the animal started from a novel location (state 10) (Fig. 5f, bottom). Each trial ended when the animal reached either end of the maze (state 4 or state 1) or failed to reach a goal within 50 steps.

Across 500 trials per random seed, incorporating offline learning significantly increased the probability of reaching the food goal in both scenarios (Fig. 5g). Moreover, among successful trials, offline learning reduced the time required to reach the food in both cases (Fig. 5h), indicating that replay-driven updates not only improved success rates but also enhanced behavioral efficiency.

The model learns aversive outcomes, predicts their presence through forward rollouts, and exhibits avoidance behavior

We next asked whether the model could also account for the learning of aversive features. This differs from reward learning (Fig. 3–5) because animals spend minimal time at aversive sites, limiting the opportunity associate the state and the outcome through prolonged dwell time. Moreover, "on-site" replay, where salience information is propagated during offline learning while the animal remains at the location, is not possible.

To simulate this, we followed the design of a previous study[9], in which mice freely explored a linear track before encountering a footshock at the track end. In our simulation, the animal completed three laps without salient outcomes (from state 1 to 8 and back), followed by a fourth lap in which a footshock occurred at state 8 (Fig. 6a). During the footshock, we simulated movement at double the normal movement speed

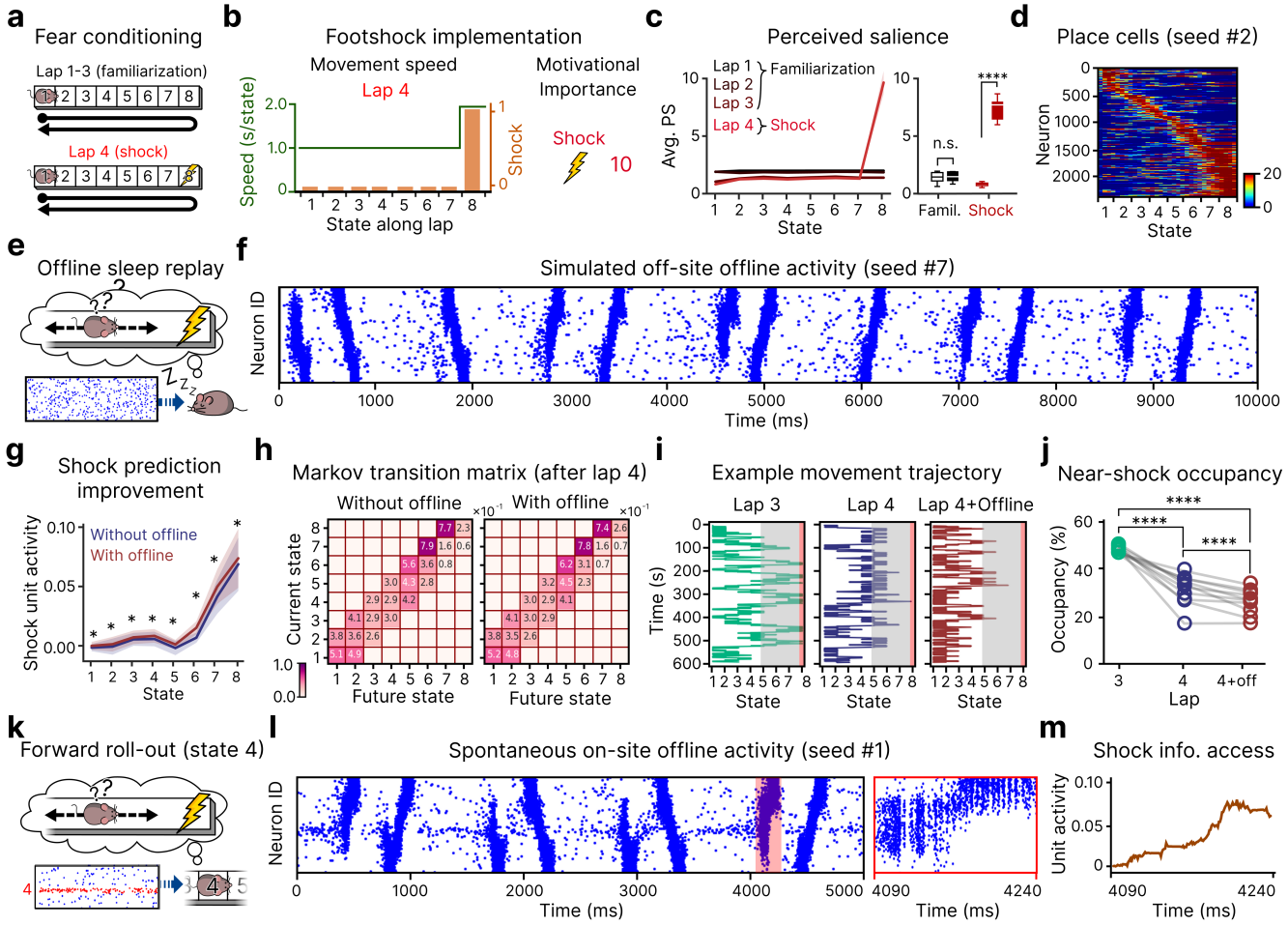

Figure 6. **a**, Aversive feature learning scheme. **b**, Two factors modulated by the introduction of aversive outcome: increased movement speed and the motivational importance of the aversive outcome. **c**, perceived salience experienced at each state on lap 1 to 4. Independent t-test, perceived salience of the non-salient states vs. perceived salience of the salient state, $N_{seed} = 10$, n.s.$P = 0.49$, ****$P = 3.41 \times 10^{-64}$. **d**, CA1 place cells clustered around the punished state, over-representing it. **e**, Offline simulation during sleep. **f**, Example spontaneously generated offline activity (10 s). **g**, Elevated anticipated footshock after the offline learning phase. Paired t-test, footshock prediction at each state without offline learning vs. with offline learning, $N_{seed} = 10$, *$P < 0.05$. **h**, Markov state transition matrices before and after the offline learning. **i**, Examples of simulated movement trajectories before footshock introduction (left), after footshock introduction without offline learning (middle), and after footshock introduction with offline learning (right). The red shaded region indicates the footshock state (state 8), and the grey shaded region indicates near-shock zone (states 5–8). **j**, Occupancy of the near-shock zone. Paired t-test, $N_{seed} = 10$, ****$P < 0.001$. **k**, Forward roll-out at state 4, simulated by inputting state 4-specific input. **l**, Left: Example spontaneously generated offline activity (5 s). Right: Zoomed-in roll-out activity. **m**, Footshock prediction output from feature-prediction layer during the roll-out activity. All data are presented as mean±s.d.

to align with rapid escape responses. Also, we treated the footshock as salient, setting its motivational importance to 10 (Fig. 6b). Compared to familiarization laps, perceived salience sharply increased at state 8 during footshock exposure (Fig. 6c), inducing over-representation of that location despite the short dwell time (Fig. 6d).

We then simulated an offline phase in which the animal was removed from the environment by providing random, low-intensity input to CA3 cells for 10 seconds (Fig. 6e). As a result, spontaneous replay-like activity emerged, spanning the entire track (Fig. 6f). We then used symmetric STDP to update W_{CA3} and W_{CA1} based on the resulting 10 seconds of simulated spiking activity.[31].

We found that incorporating offline learning extended the shock prediction field: replay enabled the shock to be predicted from locations farther away along the track (Fig. 6g). This change in prediction translated into altered behavior. With offline learning, the animal began to avoid moving toward the shock zone from more distant states, including states 2-4 (Fig. 6h). Simulations of 600-seconds of free movement further revealed that offline learning reduced the animal's occupancy of the half of the track containing the footshock state (states 5–8; the near-shock zone) (Fig. 6i). We quantified this effect by measuring near-shock zone occupancy, which was significantly decreased when offline learning was included (Fig. 6j, right), consistent with experimental findings[9].

Another important finding from the same study was that, when the mice paused as they walked toward the shock zone after reintroduction to the environment, they exhibited forward-directed replay events toward the shock zone[9]. We hypothesized that such "forward roll-outs" allow the animal to mentally access information about the footshock without physically entering the footshock state. To test this, we simulated an offline phase with place input from the middle of the track (state 4) (Fig. 6k). The network spontaneously generated sequential place cell activity extending toward both ends of the track (Fig. 6l, left), including forward roll-out events that included the footshock state (Fig. 6l, right). Consistent with our hypothesis, internal footshock prediction increased during these roll-out events (Fig. 6m).

Together, these results show that aversive stimuli can be learned reliably despite minimal exposure, highlighting distinct learning processes during behavior and offline periods that synergistically contribute to adaptive behavior.

Discussion

In this study, we introduced a unified normative theory of the cognitive map and its role in value-based decision making, bridging neural representations, learning rules and behavioral outcomes. Our framework extends the SR by incorporating SFs: CA3 encodes a salience-neutral representation of environmental structure, CA1 integrates this with salience information to form a PS-weighted SR, and a downstream feature-prediction layer computes SFs. These predicted features can then be combined with context-varying values to guide decisions. The model is learned through BTSP during online exploration and further refined by symmetric STDP during offline replay. It adapts swiftly when environmental contingencies change and captures a range of experimentally observed behaviors, linking synaptic mechanisms to network-level representations and flexible actions.

Our framework advances the seminal SR–based account of the cognitive map by explicitly separating perceived salience, feature prediction, and value assignment into distinct components. This compartmentalized structure explains why the hippocampus over-represents salient locations even when they are not intrinsically rewarding and do not necessarily lead to increased future visitation (Figs. 3 and 6). In addition, incorporating SF enables flexible integration of time-varying information such as motivational needs[10]. Because the model predicts features rather than states *per se*, it can rapidly adjust subjective value related to the features and adapt behavior based on motivational state without requiring relearning of the underlying environmental structure (Fig. 4).

Mechanistically, our work incorporates and extends prior findings on BTSP's role in driving over-representation of rewarding locations[18,21]. We further model how this over-representation may arise through different factors for rewarding versus aversive stimuli. In our simulations, positive outcomes were learned through moderate salience signals combined with prolonged occupancy (Fig. 3), whereas aversive outcomes were encoded through much stronger perceived salience despite extremely brief dwell times (Fig. 6). Our model also predicts how these over-representations accelerate learning of feature–location associations, as elevated activity at salient sites drives faster acquisition within the feature-prediction layer (Fig. 3j).

Our model proposes a unified account of replay's contribution to learning the cognitive map by linking existing findings. Recent work suggests that CA3 learns through BTSP with a symmetric time kernel[30], that symmetric recurrent weight profiles can generate spontaneous replay[31,38], and that replay contributes to consolidating SR-like representations[39]. Integrating these findings, our model captures how a symmetric, value-neutral map of environmental structure can emerge in CA3 after a few laps of exploration via symmetric BTSP, which generates spontaneous replay even in the absence of informative input (Fig. 2). These replay events, in turn, strengthened the cognitive map to facilitate earlier prediction of salient features (Fig. 5-6). Moreover, because CA3 encodes structural relationships independently of actual experience, the network can generate replay sequences along physically unexplored trajectories[27,29] (Fig. 5). This enables replay-driven inference: the salience information is propagated to states never sequentially paired with salient features and improves predictions at otherwise unrelated locations. Finally, we show that the strength of upstream input to CA3 during the offline phase, potentially modulated by the salience of the experienced state[19], controls the frequency and length of replay events (Supplementary Fig. 4). This is consistent with experimental reports

that salience boosts replay expression[40].

Our model also accounts for a role of replay in value computation that leads to adaptive behavior. Simulating the offline phase within the track, analogous to immobile periods during online exploration, produced forward roll-outs similar to those observed experimentally[9] (Fig. 6). Our model captures how these roll-outs transiently activate representations of non-current states, particularly salient ones, enabling the prediction of features and the estimation of state values required for planning[35,41,42].

In spite of the progress our model represents, important questions remain. We have made many simplifying assumptions to focus on building a conceptual bridge between levels. Future work should include additional pathways in the hippocampus, and further details of the physiological implementation of some of the functional circuit properties, both to create a more fully realized simulation and to achieve a closer fit to some aspects of neural activity observed during behavioral and replay episodes (see Supplementary Materials, Section 1). One important target for this future work will be to more fully capture how replay content is selected or modulated. Some studies suggest that replay prioritizes newly acquired salient memories, contributing to their consolidation[9,40]. Other work indicates that replay can preferentially sample trajectories that have not been recently experienced[10,27,43], potentially reinstating them to preserve older memories. Balancing these two seemingly competing functions—strengthening new salient information while maintaining previously learned material—is thought to be critical for preventing catastrophic interference during new learning[44,45]. Understanding how the hippocampal replay negotiates this balance, and how it is elicited to do so, remains an open question.

Broadening our focus, our framework also has implications for artificial intelligence (AI). Current AI systems often require large datasets and struggle with generalization, in part because their learning procedures make it difficult to extract and reuse structural regularities across tasks. In contrast, our approach suggests that rapid online learning through BTSP and offline refinement through replay may offer alternatives to standard gradient-based updates and help address these limitations[46,47]. Specifically, by separating learning about environmental structure from learning about features and assigning value to them[32], our framework enables rapid adaptation to changes in environmental contingencies and flexibility under shifts in internal motivational state. Replay further expands the scope of learning by propagating information to unvisited states, enhancing generalization without additional experience. In our T-maze simulations, for example, the network reproduced a key experimental finding[27,29] by inferring connections between unexplored paths and recovering the maze's structural layout. Finally, replay in our model emerges spontaneously, without external supervision, continually strengthening previously-acquired internal representations. This suggests a path toward AI systems that autonomously improve their internal representations during "rest" periods, thereby achieving greater efficiency and adaptability.

Finally, we foresee an exciting opportunity to incorporate our framework of an animal learning into models of human learning and memory. We propose that BTSP, enhanced by novelty and motivational state, is likely to contribute the rapid formation of replayable mental trajectories that can be reactivated during offline periods in humans. Such process could promote efficient learning and flexible application of knowledge, building cognitive maps of abstract, conceptual domains beyond the simple spatial environments studied through animal experiments. Future work will explore how these mechanisms generalize to human cognition and higher-level conceptual learning.

Taken together, our work presents a unified normative framework for the cognitive map and value-based decision making, together with a biologically grounded mechanistic account. The model captures phenomena spanning cellular, circuit, and behavioral levels, and provides a plausible explanation for how online exploration and offline replay interact to learn these representations and support rapid, flexible behavior. More broadly, this framework offers a foundation for extending these principles to more complex forms of learning, including human conceptual and abstract knowledge acquisition.

Methods

Neural network model

The hippocampal network

We modeled the hippocampal network as a two-layer spiking neural network, corresponding to the CA3 and CA1 subregions of the hippocampus, modifying and extending a simulation of exploration and replay in area CA3 from previous modeling work of Ecker et al.[31] Consistent with experimental findings, the CA3 layer included recurrent connectivity (W_{CA3}) and projected feedforward output to CA1 (W_{CA1}). Synaptic weights in both pathways were constrained between 0 and 10, initialized from a Gaussian distribution (mean = 0.01, standard deviation = 10^{-4}), and formed with a fixed connection probability of 0.1.

Both CA3 and CA1 layers contained the same number of excitatory neurons which were distributed across a small number of blocks we call 'states' tiling the simulated maze. Each state was represented by 400 neurons, with different numbers of states in the different environments we used as described below. To focus on learning processes within the hippocampus, we adopted simplifications of the inputs and plastic synapses in these brain areas. CA3 excitatory neurons were pre-specified to be place cells, with uniformly distributed place fields and spatial inputs reflecting the animal's position during online exploration, and CA1 excitatory neurons did not receive direct spatial input; instead, their place-selective responses emerged through learned W_{CA1}.

Dynamics of activity in this circuit differ between the online and offline simulation phases as described below.

Feature prediction layer

The feature prediction layer in our model aimed to provide a prediction of the physical presence of environmental features, including background, food, water, and shock. It comprised units representing the predicted presence (ψ) of each feature. These units received fully connected input from CA1 neurons via W_{pred} and allowed computation of a novelty signal (N) contributing to the modulation of the likelihood of plateau potentials in CA1 cells (See below). We interpret this network as a simplified representation of brain circuits involved in feature prediction and value computation, such as the nucleus accumbens, which forms a recurrent loop with CA1 and relays dopaminergic signals.

We now turn to our simulation of different phases of activity, again building on Ecker et al.[31] Whereas these authors used STDP during behavior to set up subsequent offline replay and did not simulate further synaptic changes during replay, we use BTSP during online behavior and STDP during replay to capture the rapid adaptation that is the focus of our work.

Online exploration

We simulated rodent's maze learning task which is commonly studied in experimental literature. On each lap, we moved a notional simulated animal along a path through the environment while training the hippocampal and feature prediction networks.

Maze exploration scenarios

We simulated three different maze learning scenarios:

- **An animal unidirectionally navigating a linear-track treadmill[18]:** Each complete rotation of the belt corresponded to a 2.4 m lap. For convenience, the track was discretized into 8 states (state 1 to 8, from left to right), each 30 cm in length. In each lap, the animal began at the leftmost state (state 1), traversed to the rightmost state (state 8), reached the end of the belt, and was returned to the starting point. Formally,

  $$\mathcal{S}_{\text{lap}} = \langle 1, 2, \ldots, 8 \rangle.$$

  The next lap began immediately after the animal returned to state 1.

- **An animal navigating a T-maze[10]:** The maze consisted of a 0.9 m vertical stem (state 1 to 3, from bottom to top), connected at its midpoint to a 2.1 m horizontal arm (state 4 to 10, from left to right, with state 7 as the intersection). In each lap, the animal began at the base of the stem (state 1), moved up to the center of the horizontal arm (state 7), and then turned left in odd-numbered laps (ending at state 4) or right in even-numbered laps (ending at state 10).

  Formally,

  $$\mathcal{S}_{\text{lap}N} = \begin{cases} \langle 1,2,3,7,6,5,4 \rangle, & \text{if } N \text{ is odd,} \\ \langle 1,2,3,7,8,9,10 \rangle, & \text{if } N \text{ is even.} \end{cases}$$

- **An animal round-tripping a linear maze[9]:** This scenario replicates an animal exploring a confined, 2.4 m segment of linear maze. The track was discretized into 8 states (state 1 to 8, from left to right), but unlike the linear treadmill, state 8 and state 1 are not connected. A single lap began with the animal at the left end (state 1), moving sequentially to the right end (state 8), and then returning back to the start (state 1). Formally,

  $$\mathcal{S}_{\text{lap}} = \langle 1, 2, \ldots, 7, 8, 7, \ldots, 1 \rangle.$$

Environmental features

In our simulation, states were associated with distinct environmental features, f. Environmental features are accompanied with their physical intensity I_f as well as motivational importance MI_f. The presence and absence of the features at each of the designated states s of a given environment were encoded as a presence vector $P(s)$ which remained constant across all positions within that state. Although real maze exploration environments contain many features, we simplified this to capture essential elements relevant to our work: background, food, water and shock.

- **Background:** Each state was assigned a state-specific background feature, which we thought of as the set of sensory cues in that state enabling the animal to distinguish the state from other ones. Since this feature is not attached to any affective value, we set the MI of this feature to be 1. When the state only has background but not other significant environmental features, the animal moves at the baseline speed, taking $T = 1$ second.

- **Food and water:** These features serves as a positive outcome in our simulation, and has MI of 3. When the animal was passing through the state with one of these features, it slowed to half the baseline speed, simulating an extended stay during reward consumption ($T = 2$ s).

- **Shock:** This feature serves as a negative outcome, with MI of 10. Once the animal enters a state where a shock occurs, it speeds up to twice the baseline speed for the shock state and subsequent states, reflecting an escape response ($T = 0.5$ s).

While stimuli can vary in intensity, for simplicity we set I_f to a constant unit value if feature f is present, so that $I_f = P_f$.

Another component attached to environmental features is novelty, denoted as $N_f(t)$. This quantity tracks the animal's subjective surprise associated with feature f, and was defined as the difference between the predicted presence and actual presence of the feature. The novelty values were updated at each timestep based on the absolute prediction error computed by the feature prediction network, ε, described in the section below on training the feature prediction network.

$$N_f(t) = \left| \varepsilon_f(t) \right| \tag{7}$$

Computation of perceived salience

The perceived salience (PS) of an environmental feature f, denoted as PS_f, represents the animal's subjective evaluation of how noticeable or memorable f is. In our simulations, PS was modulated by three factors: motivational importance MI, intensity I, and the novelty N of the environmental feature. Specifically, the perceived salience of feature f, PS_f, was then computed as:

$$PS_f(t) = (I_f + 1) \cdot MI_f \cdot N_f(t) \tag{8}$$

The added 1 in the expression $(I_f + 1)$ is a fixed offset that allows the absence of a feature to affect learning. The perceived salience of a state at time t, $PS(t)$, was computed as the sum of PS across all environmental features.

Spike train generation and activity level estimation

CA3 place fields were uniformly distributed along the x- and y-axes, with each field centered at a distinct position. Place fields were circular with a radius of 30 cm.

Spiking activity in CA3 excitatory neurons arose from two sources: external spatial input from the entorhinal cortex, $\mathcal{I}_{\text{place}}$, and recurrent input from other CA3 neurons, $\mathcal{I}_{\text{recurrent}}$. i_{place} for a CA3 neuron depended on the animal's Euclidean distance from the center of the neuron's place field and followed a Gaussian profile. The maximum value of $\mathcal{I}_{\text{place}}$ was fixed at 1 and the standard deviation of the Gaussian was chosen to be the radius of the field.

Recurrent input was computed as the sum of activities from all connected presynaptic neurons, weighted by W_{CA3}. This summed input was then passed through a sigmoid nonlinearity to yield the final recurrent drive $\mathcal{I}_{\text{recurrent},i}$ for each neuron i. For a sigmoid function

$$\sigma(x; a, b) = \frac{1}{1 + \exp[-b(x-a)]}, \tag{9}$$

the recurrent input to CA3 neuron i was defined as

$$\mathcal{I}_{\text{recurrent},i} = \sigma\left(\sum_j W_{\text{CA3},ij}\, r_j;\ a = 4,\ b = 3\right), \tag{10}$$

where $\sum_j W_{\text{CA3},ij}\, r_j$ is the weighted presynaptic activity, and a and b are the sigmoid offset and gain parameters, respectively.

Finally, the total firing rate of neuron i was given by:

$$FR_{\text{i}} = 20 \times \mathcal{I}_{\text{place,i}} + \mathcal{I}_{\text{recurrent,i}}. \tag{11}$$

CA1 excitatory neurons were modeled similarly but did not receive direct spatial input. Their firing rates were determined exclusively by feedforward input from CA3, $\mathcal{I}_{\text{feedforward}}$: the activity of CA3 presynaptic neurons was multiplied by W_{CA1} and passed through the same sigmoid nonlinearity (Eq. 9), with parameters $a = 4$ and $b = 2$. Formally, the feedforward drive to CA1 neuron j is:

$$\mathcal{I}_{\text{feedforward},j} = \sigma\left(\sum_i W_{\text{CA1},ji}\, r_i;\ a = 4,\ b = 2\right), \tag{12}$$

and the resulting firing rate is:

$$FR_j = 20 \times \mathcal{I}_{\text{feedforward},j}. \tag{13}$$

After calculating FRs of all neurons in both CA3 and CA1, we generated spike trains for each neuron using inhomogeneous poisson processes[31,33]. These spike trains were then filtered to remove spikes that violated an assumed 5 ms refractory period[31].

To reduce noise in estimation of post-synaptic signals that arises from the small scale of our network, we introduced temporal smoothing: spike trains for both CA3 and CA1 were generated at every Δt_{spike} interval, which was set to 100 ms. Neuronal activity $\mathcal{A}$ was quantified as the actual average firing rate of each neuron, calculated by dividing the total number of generated spikes by Δt_{spike}. Note that this differs from the ideal FR values in the equations above, as it reflects post-processing by both the inhomogeneous poisson process and the refractory period filter[31,38].

Training the hippocampal network using BTSP

Synaptic weight updates in the hippocampal network followed a BTSP rule, which depends on the interaction between presynaptic eligibility traces (ETs) and postsynaptic instructive signals (ISs)[21,22,30]. ETs were computed based on the spiking activity of presynaptic neurons, while ISs were driven by the postsynaptic neuron's dendritic plateau potentials (PPs). When a presynaptic spike occurred, the post-synaptic neuron's ET increased by a fixed amplitude, A_{ET}, and then decayed exponentially with a time constant $\tau_{\text{ET}} = 1000$ ms.

ISs were evoked by dendritic plateau potentials (PPs), modeled as stochastic events occurring in both CA3 and CA1 neurons. Each neuron k was assigned a plateau probability $p_{\text{plateau},k}$, updated every Δt_{spike}. At each 1 ms time step, a Bernoulli trial determined whether neuron k initiated a PP.

The plateau probability $p_{\text{plateau},k}$ was modulated by three factors: (1) the neuron's activity $\mathcal{A}_k$ of the current Δt_{spike} interval, (2) the perceived salience (PS) at the current time step, and (3) the mean activity of the entire layer, $\mathcal{A}_{\text{population}}$, which reflects layerwise inhibition and downregulates PP probability[21,22] (Supplementary Fig. 1). Formally, the plateau probability for neuron k was:

$$p_{\text{plateau},k} = \mathcal{A}_k \cdot (1 + 3 \cdot PS) \cdot (c_{\text{population}} + c_{\text{min}}). \tag{14}$$

As CA3 layer did not receive perceived salience signal, PS was set to 0 and $c_{\text{min}} = 0$ for CA3 neurons. For CA1 neurons, $c_{\text{min}} = 10^{-5}$.

The inhibitory scaling factor $c_{\text{population}}$ was:

$$c_{\text{population}} = 2\, c_{\text{max}}\, \sigma\big(\mathcal{A}_{\text{target}} - \mathcal{A}_{\text{population}}, 0, 5\big) - c_{\text{max}} \tag{15}$$

for $\mathcal{A}_{\text{population}} < \mathcal{A}_{\text{target}}$, and

$$c_{\text{population}} = 0, \tag{16}$$

otherwise. We set $c_{\text{max}} = 0.05 \times (1 + 0.5 \cdot PS)$ where PS was fixed to 0 for CA3 neurons.

When a PP occurred, the postsynaptic neuron's instructive signal increased by A_{IS} and decayed exponentially with a time constant τ_{IS}. For CA3 neurons, $A_{\mathrm{IS}} = 1.6$ and $\tau_{\mathrm{IS}} = 1000$ ms, same as τ_{ET} which allows symmetric time kernel of BTSP. On the other hand, CA1 layer's plateau potentials were modulated by perceived salience signal: $A_{\mathrm{IS}} = 0.4 \times (0.25 \cdot PS)$ and $\tau_{\mathrm{IS}} = 500$ ms for CA1 neurons, producing an asymmetric kernel[30]. BTSP-mediated synaptic updates occurred only during PP events. The BTSP update of the weights is a function of $ET \times IS$ as well as the initial value of the weight[21]. Initially weak weights undergo stronger potentiation even with smaller $ET \times IS$, whereas the weights that are already strong enough are more likely to undergo depression even with stronger ET and IS signal. Formally,

$$\Delta w_{ji} = (w_{\max} - w_{ji})\, k_{\mathrm{pos}}\, c_{\mathrm{pos}} - w_{ji}\, k_{\mathrm{neg}}\, c_{\mathrm{neg}}, \tag{17}$$

where

$$c_{\mathrm{pos}} = \frac{\sigma(ET_i \cdot IS_j; a_{\mathrm{pos}}, b_{\mathrm{pos}}) - \sigma(0; a_{\mathrm{pos}}, b_{\mathrm{pos}})}{\sigma(1; a_{\mathrm{pos}}, b_{\mathrm{pos}}) - \sigma(0; a_{\mathrm{pos}}, b_{\mathrm{pos}})}, \tag{18}$$

$$c_{\mathrm{neg}} = \frac{\sigma(ET_i \cdot IS_j; a_{\mathrm{neg}}, b_{\mathrm{neg}}) - \sigma(0; a_{\mathrm{neg}}, b_{\mathrm{neg}})}{\sigma(1; a_{\mathrm{neg}}, b_{\mathrm{neg}}) - \sigma(0; a_{\mathrm{neg}}, b_{\mathrm{neg}})}. \tag{19}$$

In our simulations, we set $k_{\mathrm{pos}} = 0.085$, $k_{\mathrm{neg}} = 0.01$, $a_{\mathrm{pos}} = 0.8$, $b_{\mathrm{pos}} = 6$, $a_{\mathrm{neg}} = 0.05$, and $b_{\mathrm{neg}} = 44.44$.

Training the feature prediction network using the delta rule

The feature prediction network was trained during the online exploration phase using the error-correcting delta rule[34]. Specifically, a synaptic weight w_{fi} connecting a CA1 neuron i and a feature unit f, was updated at each milisecond-level time step t as:

$$\Delta w_{fi}(t) = \mu \cdot \mathcal{A}_i(t) \cdot \varepsilon_f(t) \tag{20}$$

where μ is the learning rate, $\mathcal{A}_i(t)$ is the activity of neuron i and $\varepsilon_f(t)$ is the prediction error of feature f at time t. In our simulations, μ was set to 0.15×10^{-7} for the linear-track treadmill and linear maze scenarios, and 0.125×10^{-7} for the T-maze scenario. The prediction error was defined as the error between predicted presence (ψ) and the physical presence (ϕ) for that feature:

$$\varepsilon_f(t) = \psi_f(t) - \phi_f, \text{where} \tag{21}$$

$$\psi_f(t) = \sum_i \mathcal{A}_i(t) \cdot w_{ji}(t) \tag{22}$$

Finally, the novelty N associated with the feature at time step t is equal to the absolute value of the prediction error of the feature at that time step.

Offline phase

The offline simulation framework was adapted from Ecker et al.[31] Here, neurons were modeled using adaptive exponential integrate-and-fire dynamics, and synapses were modeled as conductances with biexponential kinetics (Supplementary Materials, Section 3.1 and 3.2). Hippocampal weights learned during online exploration (W_{CA3} and W_{CA1}) were carried over into the offline phase, with additional connectivity to inhibitory interneurons introduced. Spontaneous activity emerging in the CA3 and CA1 layers during this phase was then used to update W_{CA3} and W_{CA1} according to a symmetric STDP rule.

Connectivity optimization

Additional connectivity was introduced and optimized using an evolutionary algorithm, including: entorhinal cortex input to CA3 excitatory cells (EC→$\mathrm{Ext_{CA3}}$); CA3 excitatory cell to CA3 inhibitory interneuron ($\mathrm{Ext_{CA3}}$→$\mathrm{Inh_{CA3}}$); interneuron–interneuron ($\mathrm{Inh_{CA3}}$→$\mathrm{Inh_{CA3}}$); and inhibitory interneuron to excitatory cell ($\mathrm{Inh_{CA3}}$→$\mathrm{Ext_{CA3}}$). The same connectivity types were established in CA1 ($\mathrm{Ext_{CA1}}$→$\mathrm{Inh_{CA1}}$, $\mathrm{Inh_{CA1}}$→$\mathrm{Inh_{CA1}}$, $\mathrm{Inh_{CA1}}$→$\mathrm{Ext_{CA1}}$).

The optimization algorithm minimized a loss function designed to match network-level physiological targets: maintaining realistic population firing rates in excitatory cells, suppressing gamma-band (30–100 Hz) oscillations, and enhancing ripple-band oscillations in excitatory cell populations (Supplementary Materials, Section 3.3).

During the offline phase, spontaneous activity was simulated in both CA3 and CA1, with low-rate entorhinal cortex input to CA3. W_{CA3} and W_{CA1} were updated using a symmetric STDP rule throughout this period.

Training the hippocampal network using symmetric STDP

During offline phase simulations with the optimized synaptic connectivity, we recorded the spiking activity of individual neurons in the CA3 and CA1 layers. These recorded spike trains were then used to update W_{CA3} and W_{CA1} according to a symmetric spike-timing–dependent plasticity (STDP) rule.

Symmetric STDP only involves potentiating the connections which connect neurons that fire together. This occurred in the second pass through of the recorded spike trains, using a time step of 1 msec. Precisely, the update rule we used is described as follows, with $A_{\mathrm{STDP}} = 1 \times 10^{-3}$ and $\tau_{\mathrm{STDP}} = 20$ ms.

$$\Delta w = A_{\mathrm{STDP}} \cdot e^{|t_{post} - t_{pre}|/\tau_{\mathrm{STDP}}} \tag{23}$$

To simulate replay-based learning after exposure to food rewards in the T-maze (Fig. 5d), we isolated spiking activity within the temporal window corresponding to a single replay event. The learning effect was quantified by comparing the network's predictions before and after the weight update induced by each replay event (Supplementary Materials, Section 3.4). Similarly, the learning effect after the full 5-second offline simulation was also simulated and analyzed using the entire spiking activity (5e).

To simulate replay-based learning after exposure to shock in a linear track (Fig 6g), weight updates were based on all of the spiking activity across the 10-second off-line and off-site replay episode.

Estimating real-time feature unit activity during roll-out events

To estimate real-time feature unit activity in the feature prediction layer during offline replay (Fig. 6m), we used spike trains recorded during offline simulations. For each detected roll-out event, we computed CA1 firing rates using spikes within a 100 ms window preceding each time point, starting from the event's onset time. This procedure was repeated at 1 ms resolution throughout the duration of the roll-out event. Then, these CA1 firing rates were multiplied by the feature prediction weight matrix W_{FP} learned during online training to estimate feature unit activity at every time point.

Computation of successor feature activations

Here we describe how we determined the network's representations of successor features $\Psi_f(s)$ for a given feature f at any location s in the environment based on the knowledge in connection weights before or after exploration and/or replay. These quantities are shown directly for 32 evenly spaced positions s along the linear track used in simulations shown in Figures 2n and 3k,l and were also used as the basis for choosing actions in our behavioral simulations shown in Figures 4 to 6.

We first computed CA3 neuronal activity associated with position s. A position- and input-dependent firing rate for each CA3 neuron was first determined by using its specified spatial tuning function relative to the current position. This was then scaled by a factor of 0.45 to approximate the influence of recurrent input through W_{CA3}. CA1 neuronal activity was subsequently computed in the same manner as during the online exploration phase. Specifically, CA3 activity was forward-propagated through the feedforward weights W_{CA1} and passed through a sigmoid nonlinearity to obtain CA1 firing rates. Finally, feature-prediction unit activity was computed by linearly projecting CA1 activity through W_{pred}, giving estimates of predicted feature activation $\Psi_f(s)$.

Behavioral simulation

We conducted behavioral simulations using the information encoded in the network's three weight matrices W_{CA3}, W_{CA1}, and W_{FP} network to examine the effects of learning on behavior. This phase corresponds to the exploitation stage in reinforcement learning, during which the agent uses previously acquired knowledge to make choices. No weight updating occurred during these simulations. We simulated two behavioral decision-making scenarios: one involving a positive outcome in a T-maze and another involving an aversive outcome in a linear track. In both cases, we treated the behaving animal as standing at the center of one of the discrete states in the relevant environment, and as computing an estimate of $V(s)$ for the current state and for each state immediately adjacent to it in the environment. We used these $v(s)$ values to determine next state transition probabilities, and then sampled from these probabilities to transition to the next state.

To estimate $V(s)$, we first computed neuronal and feature-unit activity from the learned weights as described in the section above. The value of a given state s, denoted $V(s)$, was computed as:

$$V(s) = \sum_f \psi_f(s) \cdot v_f, \tag{24}$$

where $\psi_f(s)$ represents the predicted presence of feature f at state s, and v_f denotes the subjective value of that feature. The feature values v_f were dynamically modulated by the animal's transient motivational state. Given these computed state values, transition probabilities from each state to each other accessible state were computed using a softmax function. Specifically, given the vector of state values $\mathbf{V} = \{V_1, V_2, \ldots, V_N\}$ for the set of accessible states, transition probabilities were computed as follows:

$$P(s_{t+1} = j \mid s_t) = \frac{\exp(V_j)}{\sum_{k=1}^{N} \exp(V_k)}. \tag{25}$$

The simulated next state was determined by sampling from these probabilities.

Decision-making scenarios

- **T-maze with two goal locations and distinct rewards[10]:** Each trial began with the animal positioned at the stem of the maze (state 1) and ended when it reached either goal state (state 4 or 10). Food was located at the left end (state 4) and water at the right end (state 10), and the animal's motivational needs for these two rewards were systematically varied.

  To test the network's adaptability to different starting conditions, additional simulations were conducted in which the animal started from the right end (state 10) and traversed either toward the left end (state 4) or the stem (state 1), with food placed at state 4.

  In all cases, the animal was allowed a maximum of 50 steps per trial. Trials were terminated if the animal failed to reach a goal within this limit, and such cases were labeled as "failure to find the goal."

- **Linear track with an aversive outcome[9]**: Each trial began with the animal positioned at the left end of the track (state 1) and allowed to move freely for 600 steps. A shock stimulus was positioned at the right end of the track (state 8).

Statistical analysis

All statistical analyses were performed using custom Python code. Unless otherwise stated, data points represent independent simulation runs initialized with different random seeds (N_{seed} indicated in figure captions).

For comparisons between two conditions, we used paired t-tests as appropriate. One-sample t-tests were used when comparing a condition against a theoretical baseline.

Error bars represent mean ± standard deviation (s.d.) unless otherwise noted. Exact P values and statistical tests used are reported in the corresponding figure captions.

Acknowledgement

We thank A. Milstein (Rutgers University) and J. Magee (Howard Hughes Medical Institute) for valuable feedback on our implementation of BTSP and for their insights regarding the biological plausibility of our results. We also thank S. Jones, S. Grant, and J. Han (Stanford University) for helpful discussions during the early stages of the project. S.C. acknowledges support from the Emergent Cognitive Functions Fund, Department of Psychology, Stanford University.

References

1. Tolman, E. C. Cognitive maps in rats and men. *Psychol. Rev.* **55**, 189–208, DOI: 10.1037/h0061626 (1948).
2. Behrens, T. E. J. *et al.* What is a cognitive map? organizing knowledge for flexible behavior. *Neuron* **100**, 490–509, DOI: https://doi.org/10.1016/j.neuron.2018.10.002 (2018).
3. Rosenberg, M., Zhang, T., Perona, P. & Meister, M. Mice in a labyrinth show rapid learning, sudden insight, and efficient exploration. *eLife* **10**, e66175, DOI: 10.7554/eLife.66175 (2021).
4. Dayan, P. Improving generalization for temporal difference learning: The successor representation. *Neural Comput.* **5**, 613–624 (1993).
5. Stachenfeld, K. L., Botvinick, M. M. & Gershman, S. J. The hippocampus as a predictive map. *Nat. Neurosci.* **20**, 1643–1653, DOI: 10.1038/nn.4650 (2017).
6. Mehta, M. R., Quirk, M. C. & Wilson, M. A. Experience-dependent asymmetric shape of hippocampal receptive fields. *Neuron* **25**, 707–715, DOI: 10.1016/S0896-6273(00)81072-7 (2000).
7. Gustafson, N. J. & Daw, N. D. Grid cells, place cells, and geodesic generalization for spatial reinforcement learning. *PLOS Comput. Biol.* **7**, e1002235, DOI: 10.1371/journal.pcbi.1002235 (2011).
8. Gershman, S. J. *et al.* Explaining dopamine through prediction errors and beyond. *Nat. Neurosci.* **27**, 1645–1655, DOI: 10.1038/s41593-024-01705-4 (2024).
9. Wu, C.-T., Haggerty, D., Kemere, C. & Ji, D. Hippocampal awake replay in fear memory retrieval. *Nat. Neurosci.* **20**, 571–580, DOI: 10.1038/nn.4507 (2017).
10. Carey, A. A., Tanaka, Y. & van der Meer, M. A. A. Reward revaluation biases hippocampal replay content away from the preferred outcome. *Nat. Neurosci.* **22**, 1450–1459, DOI: 10.1038/s41593-019-0464-6 (2019).
11. Krishnan, S., Heer, C., Cherian, C. & Sheffield, M. E. Reward expectation extinction restructures and degrades ca1 spatial maps through loss of a dopaminergic reward proximity signal. *Nat. Commun.* **13**, DOI: 10.1038/s41467-022-34465-5 (2022).
12. Kutlu, M. G. *et al.* Dopamine release in the nucleus accumbens core signals perceived saliency. *Curr. Biol.* **31**, 4748–4761.e8, DOI: 10.1016/j.cub.2021.08.052 (2021). Doi: 10.1016/j.cub.2021.08.052.
13. Hollup, S. A., Molden, S., Donnett, J. G., Moser, M.-B. & Moser, E. I. Accumulation of hippocampal place fields at the goal location in an annular watermaze task. *The J. Neurosci.* **21**, 1635, DOI: 10.1523/JNEUROSCI.21-05-01635.2001 (2001).
14. Gauthier, J. L. & Tank, D. W. A dedicated population for reward coding in the hippocampus. *Neuron* **99**, 179–193.e7, DOI: https://doi.org/10.1016/j.neuron.2018.06.008 (2018).
15. Mamad, O. *et al.* Place field assembly distribution encodes preferred locations. *PLOS Biol.* **15**, e2002365– (2017).
16. Nikbakht, N. *et al.* Efficient encoding of aversive location by CA3 long-range projections. *Cell Rep.* **43**, 113957 (2024).
17. Dong, C., Madar, A. D. & Sheffield, M. E. Distinct place cell dynamics in ca1 and ca3 encode experience in new environments. *Nat. Commun.* **12**, DOI: 10.1038/s41467-021-23260-3 (2021).
18. Bittner, K. C., Milstein, A. D., Grienberger, C., Romani, S. & Magee, J. C. Behavioral time scale synaptic plasticity underlies CA1 place fields. *Science* **357**, 1033–1036 (2017).
19. Bittner, K. C. *et al.* Conjunctive input processing drives feature selectivity in hippocampal ca1 neurons. *Nat. Neurosci.* **18**, 1133–1142, DOI: 10.1038/nn.4062 (2015).

20. Balind, S. R. *et al.* Diverse synaptic and dendritic mechanisms of complex spike burst generation in hippocampal ca3 pyramidal cells. *Nat. Commun.* **10**, 1859, DOI: 10.1038/s41467-019-09767-w (2019).

21. Milstein, A. D. *et al.* Bidirectional synaptic plasticity rapidly modifies hippocampal representations. *eLife* **10**, e73046, DOI: 10.7554/eLife.73046 (2021).

22. Grienberger, C. & Magee, J. C. Entorhinal cortex directs learning-related changes in ca1 representations. *Nature* **611**, 554–562, DOI: 10.1038/s41586-022-05378-6 (2022).

23. Wilson, M. A. & McNaughton, B. L. Reactivation of hippocampal ensemble memories during sleep. *Science* **265**, 676–679, DOI: 10.1126/science.8036517 (1994). Doi: 10.1126/science.8036517.

24. Girardeau, G., Benchenane, K., Wiener, S. I., Buzsáki, G. & Zugaro, M. B. Selective suppression of hippocampal ripples impairs spatial memory. *Nat. Neurosci.* **12**, 1222–1223, DOI: 10.1038/nn.2384 (2009).

25. McNaughton, B. L. Cortical hierarchies, sleep, and the extraction of knowledge from memory, DOI: 10.1016/j.artint.2009.11.013 (2010).

26. Goto, A. & Hayashi, Y. Offline neuronal activity and synaptic plasticity during sleep and memory consolidation. *Neurosci. Res.* **189**, 29–36 (2023).

27. Gupta, A. S., van der Meer, M. A. A., Touretzky, D. S. & Redish, A. D. Hippocampal replay is not a simple function of experience. *Neuron* **65**, 695–705, DOI: https://doi.org/10.1016/j.neuron.2010.01.034 (2010).

28. Frank, L. M., Stanley, G. B. & Brown, E. N. Hippocampal plasticity across multiple days of exposure to novel environments. *The J. Neurosci.* **24**, 7681, DOI: 10.1523/JNEUROSCI.1958-04.2004 (2004).

29. Bakermans, J. J. W., Warren, J., Whittington, J. C. R. & Behrens, T. E. J. Constructing future behavior in the hippocampal formation through composition and replay. *Nat. Neurosci.* **28**, 1061–1072, DOI: 10.1038/s41593-025-01908-3 (2025).

30. Li, Y., Briguglio, J. J., Romani, S. & Magee, J. C. Mechanisms of memory-supporting neuronal dynamics in hippocampal area ca3. *Cell* **187**, 6804–6819.e21, DOI: 10.1016/j.cell.2024.09.041 (2024). Doi: 10.1016/j.cell.2024.09.041.

31. Ecker, A. *et al.* Hippocampal sharp wave-ripples and the associated sequence replay emerge from structured synaptic interactions in a network model of area ca3. *eLife* **11**, DOI: 10.7554/eLife.71850 (2022).

32. Barreto, A. *et al.* Successor features for transfer in reinforcement learning. In Guyon, I. *et al.* (eds.) *Advances in Neural Information Processing Systems*, vol. 30 (Curran Associates, Inc., 2017).

33. Galloni, A. R. *et al.* Neuromorphic one-shot learning utilizing a phase-transition material. *Proc. Natl. Acad. Sci.* **121**, e2318362121, DOI: 10.1073/pnas.2318362121 (2024). https://www.pnas.org/doi/pdf/10.1073/pnas.2318362121.

34. Widrow, B. & Hoff, J., Marcian E. Adaptive switching circuits. In *IRE WESCON Conference Record, part 4*, 96–104 (1960).

35. Davidson, T. J., Kloosterman, F. & Wilson, M. A. Hippocampal replay of extended experience. *Neuron* **63**, 497–507, DOI: 10.1016/j.neuron.2009.07.027 (2009). Doi: 10.1016/j.neuron.2009.07.027.

36. Foster, D. J. & Wilson, M. A. Reverse replay of behavioural sequences in hippocampal place cells during the awake state. *Nature* **440**, 680–683 (2006).

37. Bouton, M. E. Context and behavioral processes in extinction. *Learn. Mem.* **11**, 485–494 (2004).

38. Milstein, A. D., Tran, S., Ng, G. & Soltesz, I. Offline memory replay in recurrent neuronal networks emerges from constraints on online dynamics. *The J. Physiol.* **601**, 3241–3264, DOI: https://doi.org/10.1113/JP283216 (2023).

39. Bono, J., Zannone, S., Pedrosa, V. & Clopath, C. Learning predictive cognitive maps with spiking neurons during behavior and replays. *Elife* **12** (2023).

40. Ambrose, R. E., Pfeiffer, B. E. & Foster, D. J. Reverse replay of hippocampal place cells is uniquely modulated by changing reward. *Neuron* **91**, 1124–1136, DOI: 10.1016/j.neuron.2016.07.047 (2016). Doi: 10.1016/j.neuron.2016.07.047.

41. Johnson, A. & Redish, A. D. Neural ensembles in ca3 transiently encode paths forward of the animal at a decision point. *J. Neurosci.* **27**, 12176–12189, DOI: 10.1523/JNEUROSCI.3761-07.2007 (2007).

42. Pfeiffer, B. E. & Foster, D. J. Hippocampal place-cell sequences depict future paths to remembered goals. *Nature* **497**, 74–79, DOI: 10.1038/nature12112 (2013).

43. Gillespie, A. K. *et al.* Hippocampal replay reflects specific past experiences rather than a plan for subsequent choice. *Neuron* **109**, 3149–3163.e6, DOI: https://doi.org/10.1016/j.neuron.2021.07.029 (2021).

44. Saxena, R., Shobe, J. L. & McNaughton, B. L. Learning in deep neural networks and brains with similarity-weighted interleaved learning. *Proc. Natl. Acad. Sci. U. S. A.* **119**, e2115229119 (2022).

45. van de Ven, G. M., Siegelmann, H. T. & Tolias, A. S. Brain-inspired replay for continual learning with artificial neural networks. *Nat. Commun.* **11**, 4069 (2020).

46. Cheng, H. & Brown, J. W. Replay as a basis for backpropagation through time in the brain, DOI: 10.1101/2023.02.23.529770 (2023).

47. Sučević, J. & Schapiro, A. C. A neural network model of hippocampal contributions to category learning. *eLife* **12**, DOI: 10.7554/eLife.77185 (2023).

48. Leutgeb, S., Leutgeb, J. K., Treves, A., Moser, M.-B. & Moser, E. I. Distinct ensemble codes in hippocampal areas ca3 and ca1. *Science* **305**, 1295–1298 (2004).

49. Amaral, D. G. & Witter, M. P. The three-dimensional organization of the hippocampal formation: a review of anatomical data. *Neuroscience* **31**, 571–591 (1989).

50. O'Reilly, R. C. & McClelland, J. L. Hippocampal conjunctive encoding, storage, and recall: avoiding a trade-off. *Hippocampus* **4**, 661–682 (1994).

51. Yousuf, M., Packard, P. A., Fuentemilla, L. & Bunzeck, N. Functional coupling between ca3 and laterobasal amygdala supports schema dependent memory formation. *Neuroimage* **244**, 118563 (2021).

52. Li, M., Jiang, Y.-Q. & Sun, Q. A circuit from the basolateral amygdala to hippocampal CA3 regulates social behavior. *Curr. Biol.* **35**, 4349–4364.e5 (2025).

53. Kumaran, D., Hassabis, D. & McClelland, J. L. What learning systems do intelligent agents need? complementary learning systems theory updated. *Trends Cogn. Sci.* **20**, 512–534 (2016).

54. Buzsáki, G. & Chrobak, J. J. Temporal structure in spatially organized neuronal ensembles: a role for interneuronal networks. *Curr. Opin. Neurobiol.* **5**, 504–510 (1995).

55. Schlingloff, D., Káli, S., Freund, T. F., Hájos, N. & Gulyás, A. I. Mechanisms of sharp wave initiation and ripple generation. *J. Neurosci.* **34**, 11385–11398 (2014).

56. Ólafsdóttir, H. F., Carpenter, F. & Barry, C. Task demands predict a dynamic switch in the content of awake hippocampal replay. *Neuron* **96**, 925–935.e6 (2017).

57. McNamara, C. G., Tejero-Cantero, Á., Trouche, S., Campo-Urriza, N. & Dupret, D. Dopaminergic neurons promote hippocampal reactivation and spatial memory persistence. *Nat. Neurosci.* **17**, 1658–1660 (2014).

58. Hargreaves, E. L., Rao, G., Lee, I. & Knierim, J. J. Major dissociation between medial and lateral entorhinal input to dorsal hippocampus. *Science* **308**, 1792–1794 (2005).

59. Tsao, A. *et al.* Integrating time from experience in the lateral entorhinal cortex. *Nature* **561**, 57–62 (2018).

60. Sun, W. *et al.* Learning produces an orthogonalized state machine in the hippocampus. *Nature* **640**, 165–175 (2025).

61. Setlow, B., Schoenbaum, G. & Gallagher, M. Neural encoding in ventral striatum during olfactory discrimination learning. *Neuron* **38**, 625–636 (2003).

62. Gmaz, J. M., Carmichael, J. E. & van der Meer, M. A. Persistent coding of outcome-predictive cue features in the rat nucleus accumbens. *Elife* **7** (2018).

63. Pennartz, C. M. A., Ito, R., Verschure, P. F. M. J., Battaglia, F. P. & Robbins, T. W. The hippocampal-striatal axis in learning, prediction and goal-directed behavior. *Trends Neurosci.* **34**, 548–559 (2011).

64. Naud, R., Marcille, N., Clopath, C. & Gerstner, W. Firing patterns in the adaptive exponential integrate-and-fire model. *Biol. Cybern.* **99**, 335–347 (2008).

65. Gerstner, W., Kistler, W. M., Naud, R. & Paninski, L. *Neuronal dynamics* (Cambridge University Press, Cambridge, England, 2014).

Supplementary Materials

Suhee Cho[1,*] and James L. McClelland[1,*]

[1]Stanford University, Department of Psychology, Stanford, CA 94306, USA
[*]{suheecho,jlmcc}@stanford.edu

Contents

References 16

1 Simplifications in translating hippocampal circuits to the model 20

1.1 Architectural simplifications . . . 20
CA3 area • CA1 area • Regulation of activity in CA1 and CA3 • Feature prediction, value estimation, and computation of perceived salience

1.2 Learning simulation simplifications . . . 21

2 Pseudo code description of the online learning process using BTSP 22

3 Offline phase simulation details 23

3.1 Single cell model . . . 23

3.2 Synapse model . . . 23

3.3 Connection weight optimization . . . 23

3.4 Position decoding and replay event detection . . . 25

4 Supplementary figures 26

4.1 Details of synaptic learning rule during the online phase . . . 26

4.2 Online phase simulation using symmetric STDP . . . 27

4.3 Equilibrium properties of BTSP . . . 28

4.4 Replay frequency modulation based on perceived salience . . . 29

1 Simplifications in translating hippocampal circuits to the model

Our computational framework focuses on specific components of brain region and computation which are closely related to value-based decision making that we are interested in studying. Inevitably, this involves simplifying many anatomical, physiological, and circuit-level properties of the brain, as well as properties of the experimental paradigms and the resulting observed behavior. Further, that are some aspects of the results of our simulations differ from experimental observations, and in some cases a more complete model could produce better alignment.

Below, we outline the main simplifications made when mapping biological circuits onto our model and discuss their potential implications for improving alignment with data.

1.1 Architectural simplifications

1.1.1 CA3 area

To begin with, our model does not simulate the emergence of place cells in CA3; instead, we provide input to these cells that effectively assigns them to specific locations. In rodents, exposure to a novel environment rapidly induces CA3 neurons to develop distinct spatial and cue-related firing fields[17,48]. This process likely depends on specific upstream inputs that are omitted from our model.

One major omission is input from the dentate gyrus (DG). CA3 receives sparse projections from DG via the mossy fibers which exert a very strong excitatory influence on the CA3 neurons they synapse on[49], These have long been thought to play an important role in selecting neurons in CA3 to respond to the inputs they recieve from other areas[50], and it has been suggested that they might contribute to inducing the plateau potentials necessary for BTSP to induce place fields and cue-modulated responses in CA3[19,30]. Incorporating a DG granual cell layer could therefore provide a potential mechanism for determining which CA3 neurons become active place or cue cells.

Another important omission is grid cell input from the entorhinal cortex (EC). Grid cells provide periodic spatial basis functions, and combinations of these inputs are sufficient to generate single-peaked place fields[?,?,?]. Including EC grid input, together with DG drive, would likely provide a more realistic account of how CA3 place fields are formed during exploration.

Beyond spatial information, CA3 also receives environmental feature–related signals including their novelty and affective salience. These may arise either directly from the basolateral amygdala[51,52] or indirectly through projections from CA1 and EC[53]. Such pathways could enable CA3 neurons to develop feature-related receptive fields alongside spatial ones.

Taken together, DG input, EC grid input, and other modulatory signals may support a richer cognitive map within CA3, allowing neurons to form multiple fields (both spatial and feature-based). This, in turn, could allow CA3 populations to represent spatial positions and features in partially distinct subpopulations, with recurrent synaptic strengths reflecting learned place–feature associations.

A likely downstream consequence of the place–feature associations in CA3 is their likely influence on replay content. Because CA3 is a primary generator of hippocampal replay and sharp-wave ripples[?,54,55], combining spatial and feature-related inputs would be expected to bias replay toward trajectories involving salient or behaviorally significant locations[9,56]. One potential mechanism for the replay content modulation involves residual dopaminergic or neuromodulatory signals that persist during brief rest periods when the animal remains in the environment. Such signals have been shown to enhance excitability of neurons associated with salient states[57], increasing their likelihood of participating in replay.

1.1.2 CA1 area

One major omission in our CA1 implementation is the set of inputs it receives from the EC. CA1 integrates position and reward-related information from medial and lateral entorhinal regions, which convey both spatial structure and nonspatial feature cues[58,59]. Together with the environmental-feature–specific inputs described above, these signals may contribute to the development of "reward cells" in CA1 that fire selectively at the reward location[14]. Unlike standard place cells, their firing fields shift to the new reward position when the reward is relocated[14].

We further propose that the increasing specialization of CA1 neurons, driven by spatial, reward-related, and cue-specific inputs, may contribute to population-level orthogonalization based on task structure[60]. In this view, CA1 ensembles do more than represent spatial environmental structure. Rather, they progressively differentiate their activity patterns according to task-relevant cues, such as contextual cues that signal the current behavioral contingency[60]. Such task-dependent orthogonalization may reduce interference across task states that share similar spatial structure but differ in behavioral demands.

1.1.3 Regulation of activity in CA1 and CA3

Another area for refinement in our model is the fuller inclusion of physiological mechanisms for regulating neural activity, plateau potentials, and the resulting formation and activation of place cells. Below we mention two aspects of the results of our simulations that might better align with neural data by including such mechanisms:

- In experiments, place cells formed in reward zones tend to have narrower receptive fields than those in non-reward zones[22]. In contrast, in our simulations we find that the place fields formed around these zones tend to have larger larger

receptive fields than those in non-reward zones (See Figure 3f). Mechanisms that more strongly regulate how many CA1 neurons can be active at the same time might contribute to better capturing the details of the experimental observations.

- We found large differences in the frequency of replay events and the amount of activity within these events in our replay simulations (compare Figures **??**f and 5b. While the features of natural replay events certainly differ from setting to setting, these differences suggest to us that there is room for improvement in the regulation of neural activity within replay events that would keep these variations within bounds.

1.1.4 Feature prediction, value estimation, and computation of perceived salience

Outside of the hippocampus, our model simplifies the downstream structures involved in feature prediction in single "feature prediction layer" and simply specifies mathematical expressions for using variables represented in this layer to compute value and perceived salience. Although multiple interconnected regions contribute to these computations in reality, we do not implement the full mechanisms of these downstream circuits because our primary focus is the hippocampal learning mechanism.

A plausible biological substrate for the feature-prediction component of our framework is the nucleus accumbens (NAc). Prior studies suggest that NAc encodes predictions about upcoming cues and outcomes and integrates motivationally significant information relevant for reinforcement learning[61,62]. Importantly, NAc is reciprocally connected with the hippocampus: it receives dense glutamatergic projections from CA1 conveying spatial context and salient event information[63], and it can in turn modulate hippocampal processing through feedback pathways. Within our proposed framework, projections from CA1 to NAc could transmit salience-weighted spatial and feature signals, enabling NAc circuits to compute successor-feature predictions. Conversely, NAc could send novelty or prediction error signals back to CA1, helping to update the perceived salience-weighted successor representation.

Aside from NAc, there are multiple different brain subregions that can contribute to predict successor features, merge those predictions with feature-specific reward information and translate it into adaptive, subsequent behaviors.

Of course, NAc is not the only region likely to contribute. Structures such as the orbitofrontal cortex (OFC), ventral pallidum, and ventral tegmental area (VTA) have been implicated in computing or relaying feature-specific predictions, encoding state–space structure, and providing value- or novelty-related teaching signals[?,?,?]. These regions could work with hippocampus–NAc interactions to support flexible feature prediction and value computation. In summary, while our model abstracts these diverse downstream systems into a single feature-prediction module, future work incorporating their specific circuit dynamics may yield a more complete mechanistic account of how hippocampal representations guide adaptive behavior.

1.2 Learning simulation simplifications

A further simplification in our model concerns the offline simulations, particularly the on-track rest period during which replay events occur (on-site replay). In our simulations, offline activity was generated using an adaptive leaky-integrate-and-fire model, which incorporates firing-rate adaptation such that neurons active immediately before an offline epoch become less likely to fire. This mechanism has been proposed to influence replay directionality by biasing propagation away from recently active neurons[29,31].

However, in our implementation, the firing activity from the end of the online exploration phase was not carried over into the subsequent offline simulation. Incorporating this continuity may help explain a broader range of experimental findings regarding replay content. For example, Wu et al. showed that when an animal pauses along the way to a salient aversive location, replay preferentially propagates forward toward the shock site[9]. If recent neural activity were inherited across phases, neurons representing positions just behind the animal (ones farther from the shock) would be less likely to participate in replay due to recent firing-induced adaptation, whereas neurons coding positions ahead (including the shock zone) would remain more excitable. This carryover mechanism may therefore help account for preferential forward replay toward salient outcomes during on-site pauses.

2 Pseudo code description of the online learning process using BTSP

The complete online learning process is described as Algorithm 1 below.

Algorithm 1: Training during online environment exploration

```
Input  : S_lap, I_s, P_s, MI
Output : W_CA3, W_CA1, W_pred

Initialize:
    # Initialize weights and signals.
    W_CA3 ~ N(10^-2, 10^-8); W_CA1 ~ N(10^-2, 10^-8); W_pred ← 0
    A_CA3 ← 0; ET ← 0; IS_CA3 ← 0; IS_CA1 ← 0

for lap = 1 to Totallaps do
    for s ∈ S_lap do
        for t = 1 to T_s do
            # Generate new spike trains and calculate the activities at every
              T_SpikeUpdate.
            if mod(t, T_SpikeUpdate) = 0 then
                SpikeTrain_CA3 ← GenerateSpikeTrain(s, A_CA3, W_CA3)
                A_CA3 ← Activity(SpikeTrain_CA3)

                SpikeTrain_CA1 ← GenerateSpikeTrain(·, A_CA3, W_CA1)
                A_CA1 ← Activity(SpikeTrain_CA1)
            end

            # Compute novelty and train the feature prediction network.
            (N(t), W_pred) ← DeltaRule(P_s, A_CA1, W_pred)
            PS(t) ← PerceivedSalience(I_s, N(t), MI)

            # Calculate the plateau probability of hippocampal neurons.
            p_plataeu,CA3 ← PlateauProbability(A_CA3, ·)
            p_plataeu,CA1 ← PlateauProbability(A_CA1, PS(t))

            # Update ETs and ISs.
            ET += UpdateET(SpikeTrain_CA3)
            IS_CA3 += UpdateIS(p_plataeu,CA3)
            IS_CA1 += UpdateIS(p_plataeu,CA1)

            # Train the hippocampal network.
            W_CA3 ← BTSP(ET, IS_CA3, W_CA3)
            W_CA1 ← BTSP(ET, IS_CA1, W_CA1)

            # Decay eligibility traces and instructive signals.
            ET -= ET/τ_ET
            IS_CA3 -= IS_CA3/τ_IS_CA3
            IS_CA1 -= IS_CA1/τ_IS_CA1
        end
    end
end
```

3 Offline phase simulation details

Offline-phase simulations were performed using python library Brian 2[?], using the synaptic weight matrices W_{CA3} and W_{CA1} obtained from the online learning phase. Starting from these learned weights, we adopted the offline simulation framework of Ecker et al.[31], using their publicly available code as the basis for our implementation.

3.1 Single cell model

We used a neuron model with the adaptive exponential integrate-and-fire (AdExIF) equations[64,65], as in Ecker et. al[31]. Here, the membrane potential $V(t)$ and adaptation current $w(t)$ interact, following the equations:

$$C_m \frac{dV(t)}{dt} = -g_L(V(t) - V_{\mathrm{rest}}) + g_L \Delta_T \exp\left(\frac{V(t) - \vartheta}{\Delta_T}\right) - w(t) + I_{\mathrm{syn}}(t), \tag{26}$$

$$\tau_w \frac{dw(t)}{dt} = a(V(t) - V_{\mathrm{rest}}) - w(t). \tag{27}$$

When $V(t)$ crosses the threshold ϑ, it is reset to V_{reset} and held for a refractory period t_{ref}. The model incorporates adaptation process, which is important in replay generation[31]. The adaptation current $w(t)$ is incremented by b at each spike, where a and b control subthreshold and spike-triggered adaptation, respectively.

The actual parameter values used for the simulations are summarized in Table 1, adapted from the previous work[31]. Physical units are as follows: C_m (pF), g_L and a (nS), V_{rest}, Δ_T, ϑ, and V_{reset} (mV), t_{ref} and τ_w (ms), and b (pA).

Table 1. Neuron model parameters.

Parameter	Symbol	Value
Membrane capacitance	C_m	180.13
Leak conductance	g_L	5
Leak reversal (resting) potential	V_{rest}	-75.19
Slope of exponential term	Δ_T	4.23
Firing threshold	ϑ	-24.42
Adaptation time constant	τ_w	84.93
Subthreshold adaptation strength	a	-0.01
Spike-triggered adaptation increment	b	500
Reset potential	V_{reset}	-29.74
Absolute refractory period	t_{ref}	5.96

3.2 Synapse model

Synapses were modeled as conductances with biexponential kinetics:

$$g(t) = \hat{g}A\left[\exp\left(-\frac{t}{\tau_d}\right) - \exp\left(-\frac{t}{\tau_r}\right)\right], \tag{28}$$

where $\hat{g}$ is the peak conductance, and τ_r and τ_d are the rise and decay time constants, respectively.

The normalization constant $A = \exp(-t_p/\tau_d) - \exp(-t_p/\tau_r)$ ensures that the conductance peaks at time $t_p = \tau_r\tau_d/(\tau_d - \tau_r)\ln(\tau_d/\tau_r)$. Synaptic currents were computed as

$$I_{\mathrm{syn}}(t) = g_{\mathrm{AMPA}}(t)\,(V(t) - E_{\mathrm{exc}}) + g_{\mathrm{GABA}}(t)\,(V(t) - E_{\mathrm{inh}}), \tag{29}$$

where $E_{\mathrm{exc}} = 0$ mV and $E_{\mathrm{inh}} = -70$ mV are the reversal potentials of excitatory and inhibitory synapses, respectively.

The parameters used for the synapses are summarized in Table 2. Ext stands for excitatory cells, Inh stands for inhibitory cells, and EC stands for entorhinal cortex populations. Physical dimensions are as follows: $\hat{g}$ (nS), τ_r, τ_d, and t_d (ms), and connection probability p_{conn} is dimensionless.

3.3 Connection weight optimization

Synaptic weights of the network were optimized using the publicly available code from the previous study[31] after being modified to incorporate W_{CA1} network. We sought to determine an optimal set of single-valued parameters determining the strength of excitatory and inhibitory connections within and between hippocampal subfields. Specifically, the parameters optimized are listed below:

Table 2. Synaptic parameters (adapted from[31]).

Connection	$\hat{g}$ (nS)	τ_r (ms)	τ_d (ms)	t_d (ms)	p_{conn}
Ext → Ext	0.1-6.3	0-15	1.3	9.5	0.1
Ext → Inh	0.85	1.0	4.1	0.9	0.1
Inh → Ext	0.65	0.3	3.3	1.1	0.25
Inh → Inh	5.0	0.25	1.2	0.6	0.25
EC → Ext	19.15	21.5	5.4	–	–

- Entorhinal cortex (EC) input rate
- EC → CA3 excitatory connection weight
- CA3 excitatory → CA3 inhibitory connection weight
- CA3 inhibitory → CA3 excitatory connection weight
- CA3 inhibitory → CA3 inhibitory connection weight
- Weight scaling factor for W_{CA3}
- CA1 excitatory → CA1 inhibitory connection weight
- CA1 inhibitory → CA1 excitatory connection weight
- CA1 inhibitory → CA1 inhibitory connection weight

Optimization followed the evolutionary multi-objective framework[31], with customized upper and lower bounds for each parameter listed in Table 3. The final optimized weights used in the three task environments are summarized in Table 4.

Table 3. Upper bound and lower bound values used for the optimization process.

Parameter	Lower bound	Upper bound
EC input rate	5.0	15.0
EC → CA3 Ext	0.5	40.0
CA3 Exc → Inh	0.2	5.0
CA3 Inh → Exc	0.5	20.0
CA3 Inh → Inh	1.0	15.0
CA3 weight scale (W_{CA3})	1.0	2.5
CA1 Exc → Inh	0.2	5.0
CA1 Inh → Exc	1.0	10.0
CA1 Inh → Inh	1.0	15.0

Table 4. Optimized connection weights. Each value represents the final parameter obtained after evolutionary optimization.

Parameter	Linear treadmill	T-maze	Closed linear track
EC input rate	10.084	7.322	13.038
EC → CA3 Ext	23.957	34.481	15.843
CA3 Exc → Inh	0.349	1.765	1.715
CA3 Inh → Exc	1.941	1.381	1.646
CA3 Inh → Inh	2.971	11.110	14.732
CA3 weight scale (W_{CA3})	2.210	1.886	2.306
CA1 Exc → Inh	1.000	1.765	0.337
CA1 Inh → Exc	1.198	1.877	1.052
CA1 Inh → Inh	14.725	13.819	12.671

3.4 Position decoding and replay event detection

Using the simulated spontaneous activity of CA3 neurons during the offline phase, we detected individual replay events following the spatial position decoding procedure described by Davidson et al.[35].

We first identified candidate replay periods as time blocks in which the mean firing rate of the CA3 population exceeded 2 Hz for at least 200 ms. Only these high-activity periods were considered for subsequent decoding analysis.

For each candidate event, we defined a set of possible decoded positions along the trajectory of interest. These positions were defined by subdividing each behavioral state into four equally spaced spatial points. For example, when analyzing shortcut replay events (Fig. 5), states 4–10 were included, resulting in a total of 28 candidate spatial positions.

CA3 firing rates were computed in sliding 10 ms time windows across the candidate replay event. For each time bin, we estimated the posterior probability of the animal being at each candidate position by comparing the observed CA3 firing rates with the ideal spatial tuning curves of each CA3 neuron (see Methods). As a result, a posterior probability matrix $X_{\text{posterior}}$ was obtained, indexed by spatial position and time.

To quantify whether the decoded activity formed a coherent sequential trajectory, we fitted a straight line to the posterior matrix, assuming a constant-velocity traversal through space. The "goodness" of fit of this line was quantified using the metric R, adapted from Davidson et al.[35]. Specifically, R measures the fraction of posterior probability mass being included within a narrow band surrounding the fitted line:

$$R = \frac{\sum_{x,t} X_{\text{posterior}}(x,t)\,\mathbb{I}\big(|x-\hat{x}(t)| < d\big)}{\sum_{x,t} X_{\text{posterior}}(x,t)},$$

where $\hat{x}(t)$ denotes the position predicted by the fitted line at time t, $\mathbb{I}$ is an indicator function, and d is a spatial tolerance (band size). To ensure that the fitted trajectory spanned a meaningful portion of the spatial domain, we required that the fitted line pass through at least one-third of the spatial bins; otherwise, R was set to zero.

To assess statistical significance, we generated a null distribution by repeating the same decoding procedure 100 times using shuffled CA3 spatial tuning curves. A candidate event was classified as a valid replay if its true R value exceeded the 95th percentile of the shuffled R distribution. The slope and intercept of the fitted line were then used to classify replay direction and trajectory type.

4 Supplementary figures

4.1 Details of synaptic learning rule during the online phase

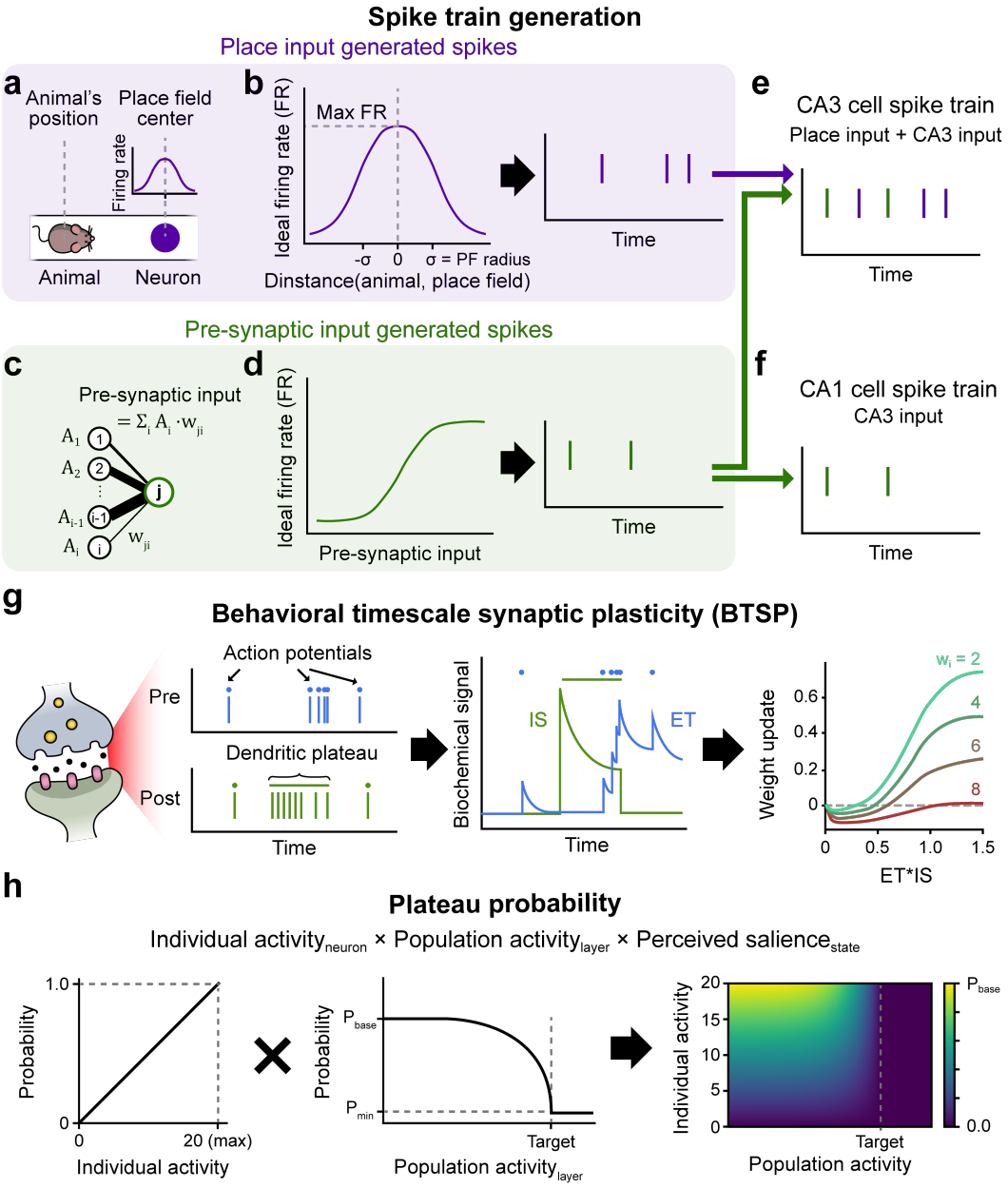

Supplementary Figure 1. Spiking neural network model activity. **a–f**, Spike-generation process. **a**, Place-input–driven firing rates were determined by the distance between the animal and each place cell's field center. **b**, This distance was converted to a firing rate using a Gaussian tuning curve. **c**, Pre-synaptic input–driven firing rates were computed from the weighted sum of pre-synaptic activity. **d**, The weighted sum was passed through a sigmoid nonlinearity to obtain the final rate. **e**, CA3 cell firing rates were computed as the sum of place-input–generated and pre-synaptic–input–generated components. **f**, CA1 cell firing rates were determined solely by pre-synaptic–input–generated activity. **g**, Behavioral time-scale synaptic plasticity (BTSP). Each pre-synaptic action potential produced an eligibility trace (ET), and each post-synaptic dendritic plateau potential (PP) generated an instructive signal (IS). Synaptic weight updates depended on the product of ET and IS. **h**, Modulation of PP probability. In our model, the probability of PP occurrence was computed as the product of a neuron's recent activity, population-level normalization, and the perceived salience of the current state.

4.2 Online phase simulation using symmetric STDP

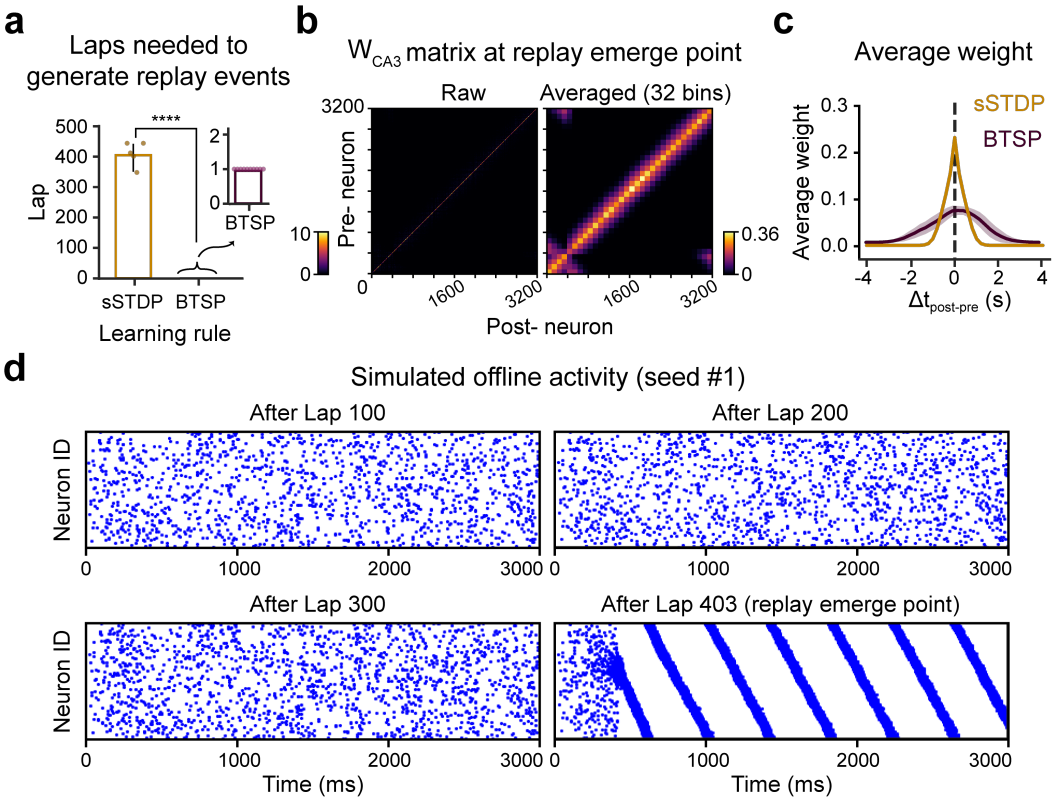

Supplementary Figure 2. Laps the animal needs to travel for its CA3 network to acquire spontaneously-generated reply activity, in the linear-treadmill simulations. **a**, Replay emerge point, defined by the number of laps needed to generate spontaneous replays. The networks trained with symmetric STDP (sSTDP) demonstrated much later emergence of replay, compared to one-shot acquisition of replay within the networks trained using BTSP. **b**, W_{CA3} of a network trained using sSTDP at the replay emerge point. Left: W_{CA3}, Right: Averaged W_{CA3} computed by dividing the matrix into 32 bins and computed, plotted averaged value of each bin. **c**, Average connection weight profile of networks trained by sSTDP and BTSP. sSTDP trained weights showed stronger connection weight to other CA3 place cells with nearby place fields. BTSP trained weights are projected more broadly, projecting weights to place cells with far place fields and less strong connections to cells with nearby place fields. **d**, Simulated offline phase of sSTDP trained network. Before the replay emerge point, the activity does not show significant clustered firing or replay like activity. At lap 403 which is its replay emerge point, replay activity emerge.

4.3 Equilibrium properties of BTSP

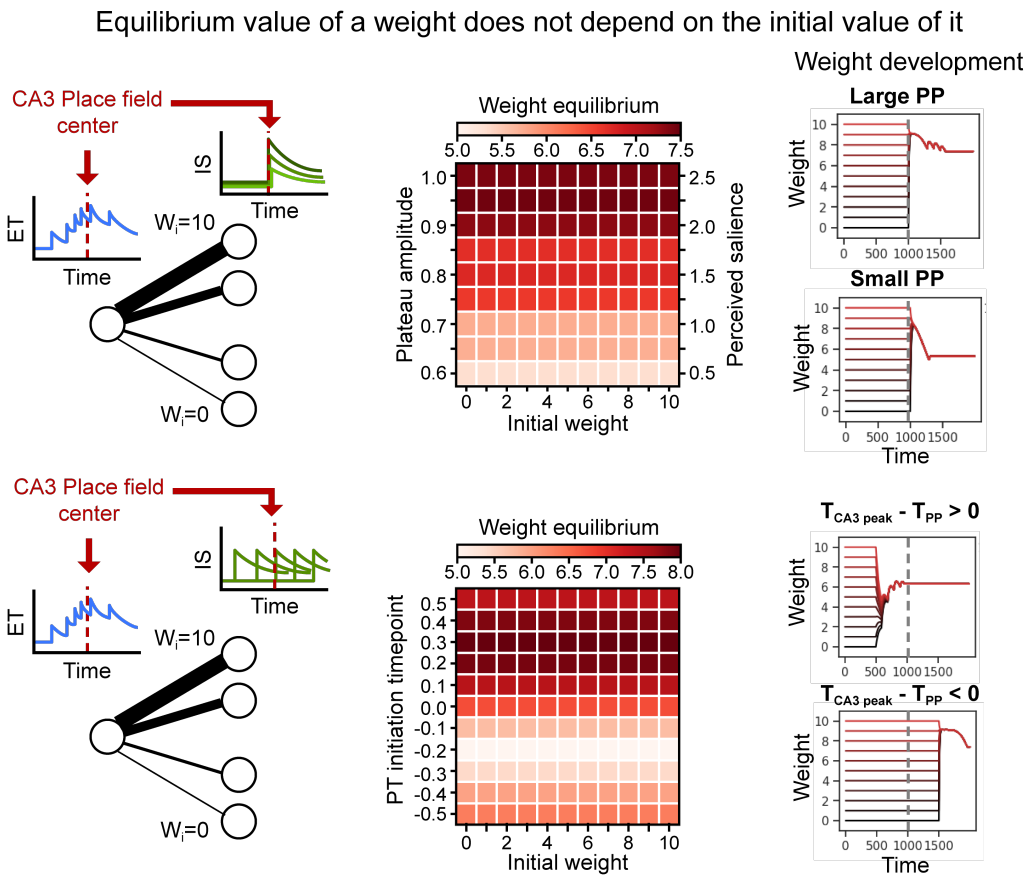

Supplementary Figure 3. Simulations of synaptic weight updates as a function of plateau amplitude (top) and plateau onset timing (bottom), across different initial synaptic weight strengths. The results show that the final synaptic weights are modulated by plateau amplitude and onset timing, but not by the initial synaptic weight value.

4.4 Replay frequency modulation based on perceived salience

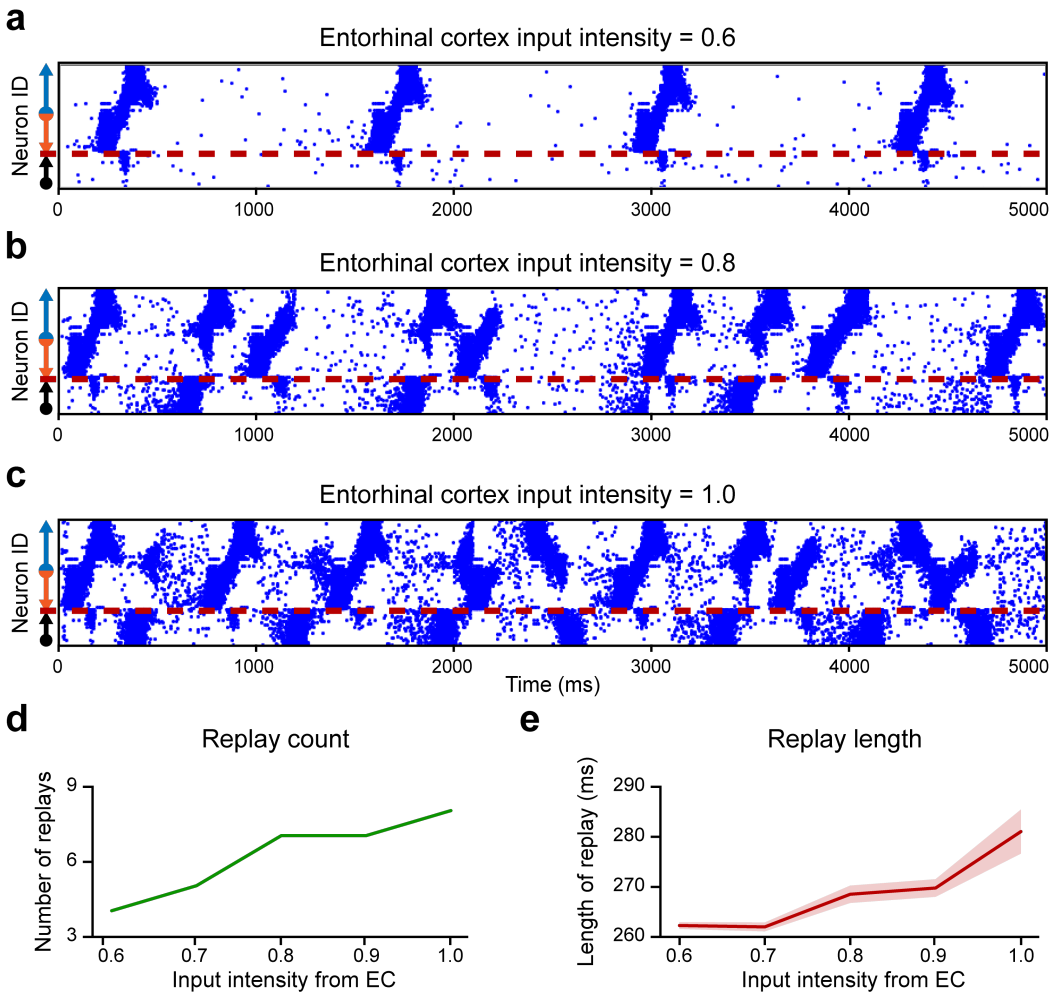

Supplementary Figure 4. Replay frequency and event length are modulated by the strength of entorhinal cortex (EC) input. **a–c**, Simulated offline activity in networks that learned the T-maze task under different EC input strengths (related to Fig. 4–5). **a**, EC input at 60% of the standard strength. **b**, EC input at 80% of the standard strength. **c**, EC input at 100% (full) strength. **d**, Number of replay events as a function of EC input strength. **e**, Replay event length as a function of EC input strength.

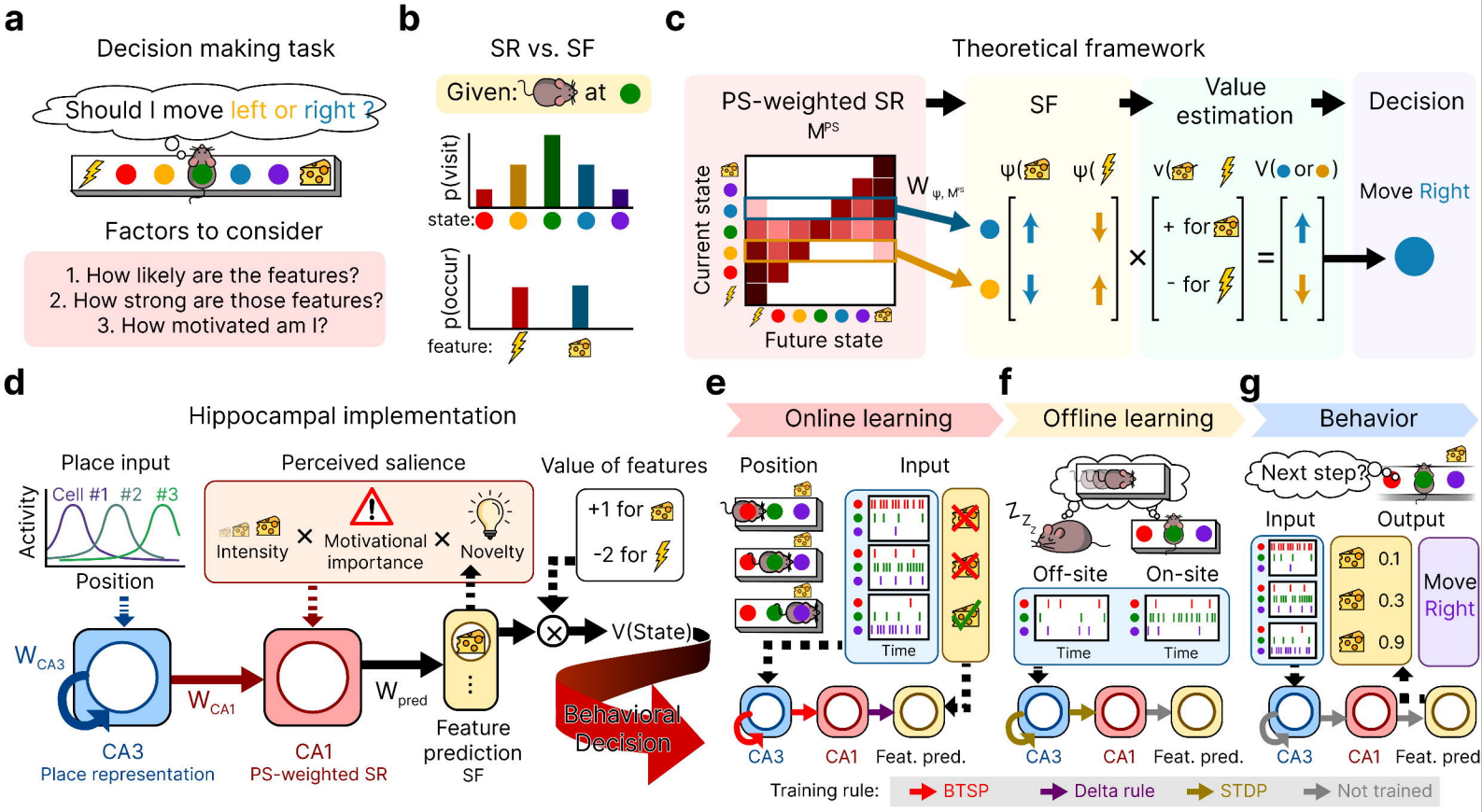
a
Decision making task
Should I move left or right ?
Factors to consider
1. How likely are the features?
2. How strong are those features?
3. How motivated am I?
b
SR vs. SF
Given: at
p(visit)
state:
p(occur)
feature:
c
Theoretical framework
PS-weighted SR
M^{PS}
Current state
Future state
$W_{\psi, M^{PS}}$
SF
Value estimation
Decision
Move Right
+ for
- for
d
Hippocampal implementation
Place input
Cell #1 #2 #3
Activity
Position
Perceived salience
Intensity
Motivational importance
Novelty
Value of features
+1 for
-2 for
W_{CA3}
W_{CA1}
W_{pred}
V(State)
CA3
Place representation
CA1
PS-weighted SR
Feature prediction
SF
Behavioral Decision
e
Online learning
Position
Input
Time
CA3
CA1
Feat. pred.
f
Offline learning
Off-site
On-site
Time
g
Behavior
Next step?
Input
Output
0.1
0.3
0.9
Move Right
Training rule:
BTSP
Delta rule
STDP
Not trained

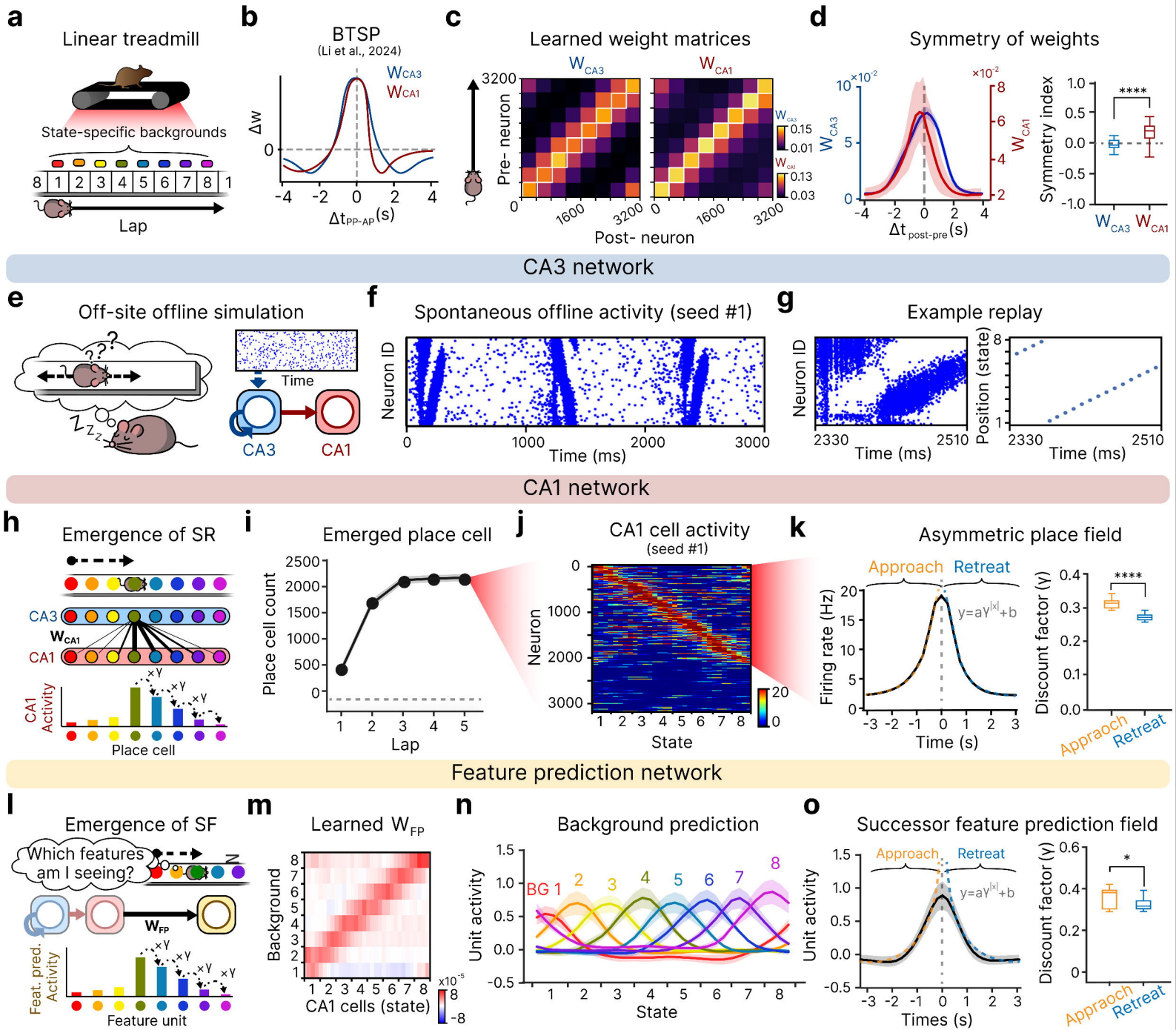
a
Linear treadmill
State-specific backgrounds
8 1 2 3 4 5 6 7 8 1
Lap
b
BTSP
(Li et al., 2024)
W_CA3
W_CA1
Δw
Δt_PP-AP(s)
c
Learned weight matrices
W_CA3
W_CA1
Pre- neuron
Post- neuron
d
Symmetry of weights
W_CA3
W_CA1
Δt_post-pre (s)
Symmetry index
****
CA3 network
e
Off-site offline simulation
Time
CA3
CA1
f
Spontaneous offline activity (seed #1)
Neuron ID
Time (ms)
g
Example replay
Neuron ID
Time (ms)
Position (state)
Time (ms)
CA1 network
h
Emergence of SR
CA3
W_CA1
CA1
CA1 Activity
Place cell
i
Emerged place cell
Place cell count
Lap
j
CA1 cell activity
(seed #1)
Neuron
State
k
Asymmetric place field
Approach
Retreat
y=aγ^|x|+b
Firing rate (Hz)
Time (s)
Discount factor (γ)
****
Appraoch
Retreat
Feature prediction network
l
Emergence of SF
Which features am I seeing?
W_FP
Feat. pred. Activity
Feature unit
m
Learned W_FP
Background
CA1 cells (state)
n
Background prediction
BG 1
Unit activity
State
o
Successor feature prediction field
Approach
Retreat
y=aγ^|x|+b
Unit activity
Times (s)
Discount factor (γ)
*
Appraoch
Retreat

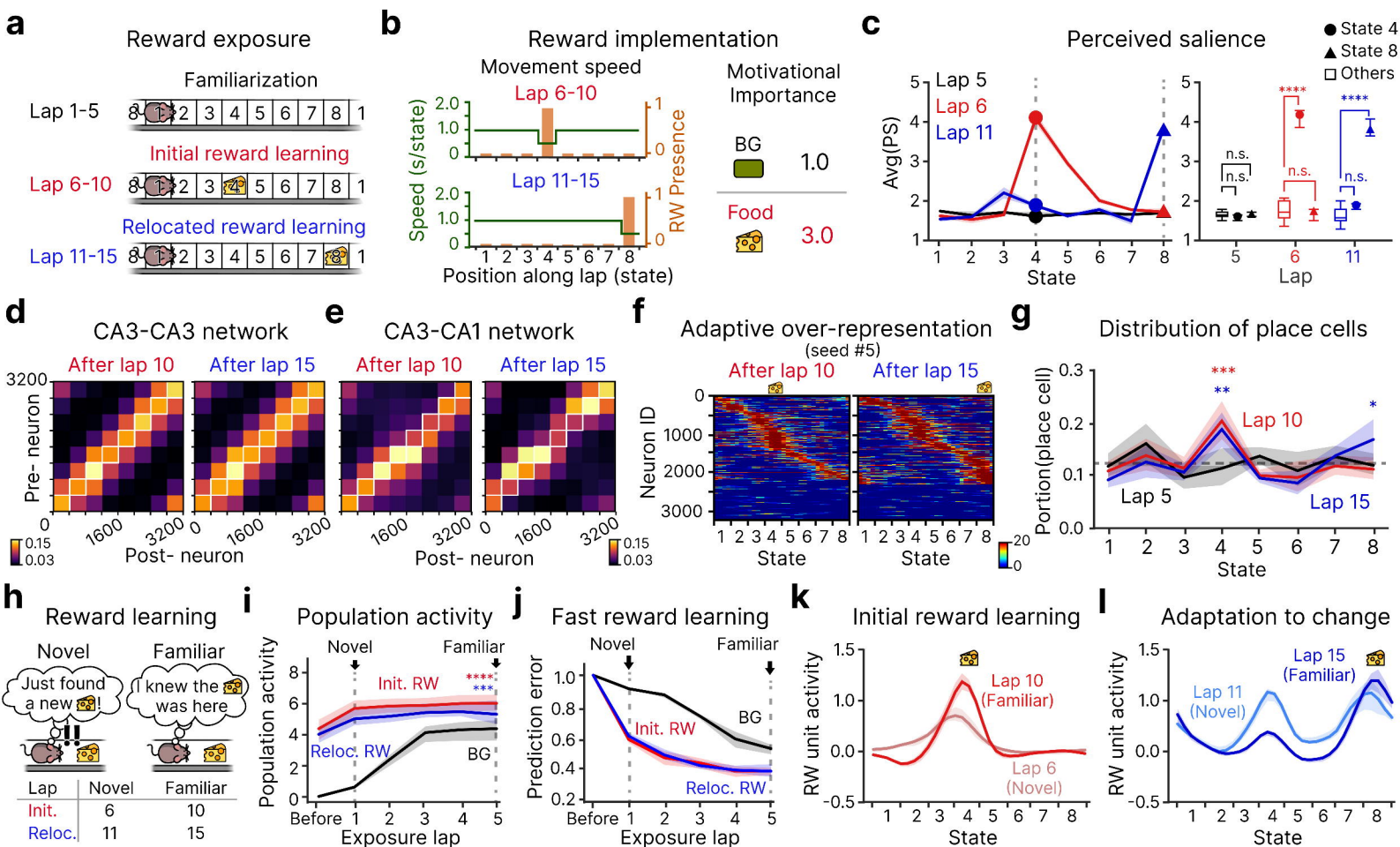
a
Reward exposure
Familiarization
Lap 1-5
Initial reward learning
Lap 6-10
Relocated reward learning
Lap 11-15
b
Reward implementation
Movement speed
Lap 6-10
Lap 11-15
Speed (s/state)
RW Presence
Position along lap (state)
Motivational Importance
BG
1.0
Food
3.0
c
Perceived salience
State 4
State 8
Others
Lap 5
Lap 6
Lap 11
Avg(PS)
State
Lap
n.s.
****
d
CA3-CA3 network
After lap 10
After lap 15
Pre- neuron
Post- neuron
e
CA3-CA1 network
f
Adaptive over-representation
(seed #5)
Neuron ID
State
g
Distribution of place cells
Portion(place cell)
Lap 10
Lap 5
Lap 15
***
**
*
h
Reward learning
Novel
Familiar
Just found a new !
I knew the was here
Lap
Novel
Familiar
Init.
6
10
Reloc.
11
15
i
Population activity
Novel
Familiar
Init. RW
Reloc. RW
BG
Exposure lap
j
Fast reward learning
Prediction error
k
Initial reward learning
RW unit activity
Lap 10 (Familiar)
Lap 6 (Novel)
l
Adaptation to change
Lap 11 (Novel)
Lap 15 (Familiar)

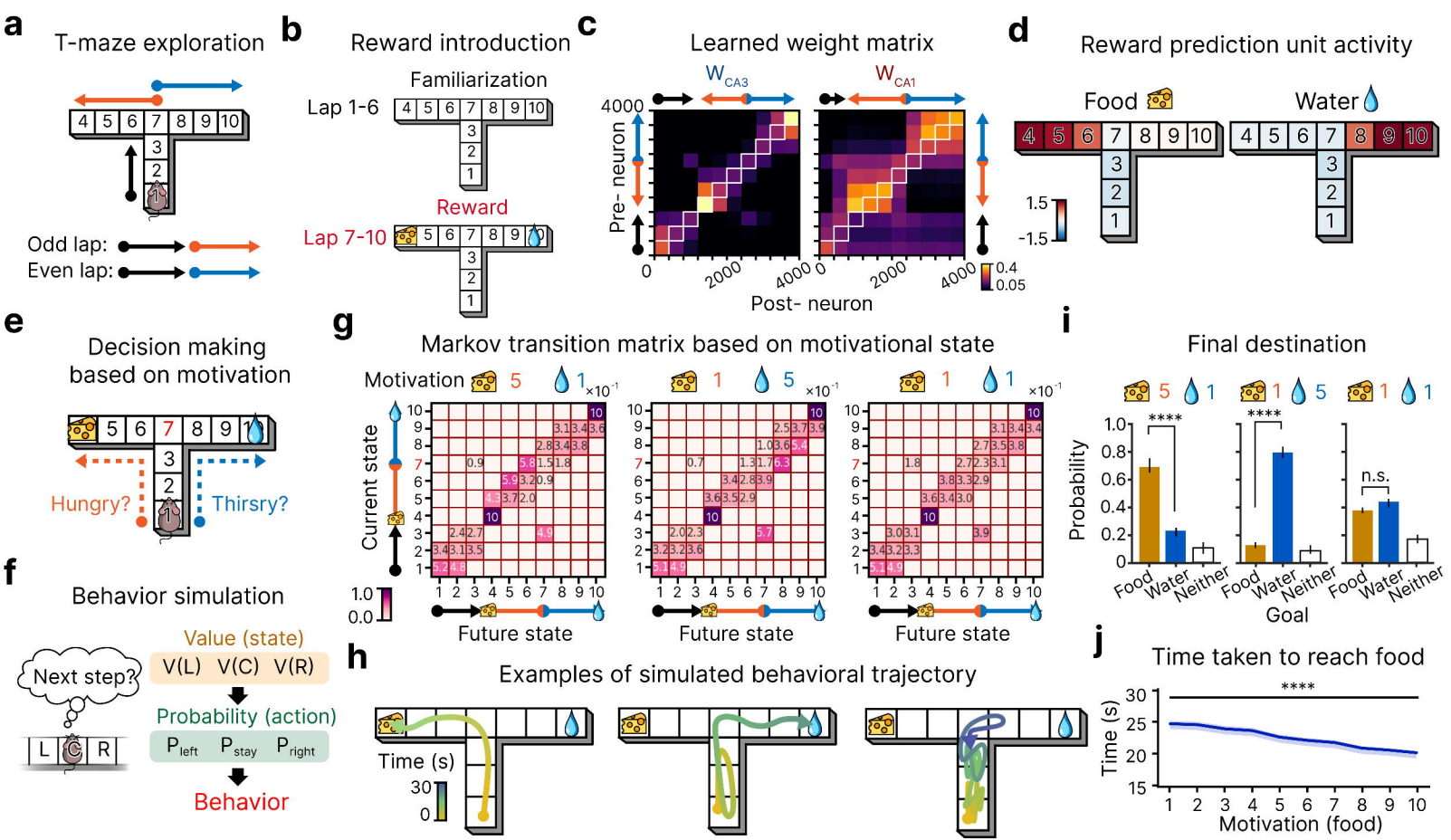
a
T-maze exploration
Odd lap:
Even lap:
b
Reward introduction
Familiarization
Lap 1-6
Reward
Lap 7-10
c
Learned weight matrix
W_{CA3}
W_{CA1}
Pre- neuron
Post- neuron
d
Reward prediction unit activity
Food
Water
e
Decision making based on motivation
Hungry?
Thirsry?
f
Behavior simulation
Next step?
Value (state)
V(L) V(C) V(R)
Probability (action)
P_{left} P_{stay} P_{right}
Behavior
g
Markov transition matrix based on motivational state
Motivation
Current state
Future state
h
Examples of simulated behavioral trajectory
Time (s)
i
Final destination
Probability
Food
Water
Neither
Goal
n.s.
j
Time taken to reach food
Time (s)
Motivation (food)

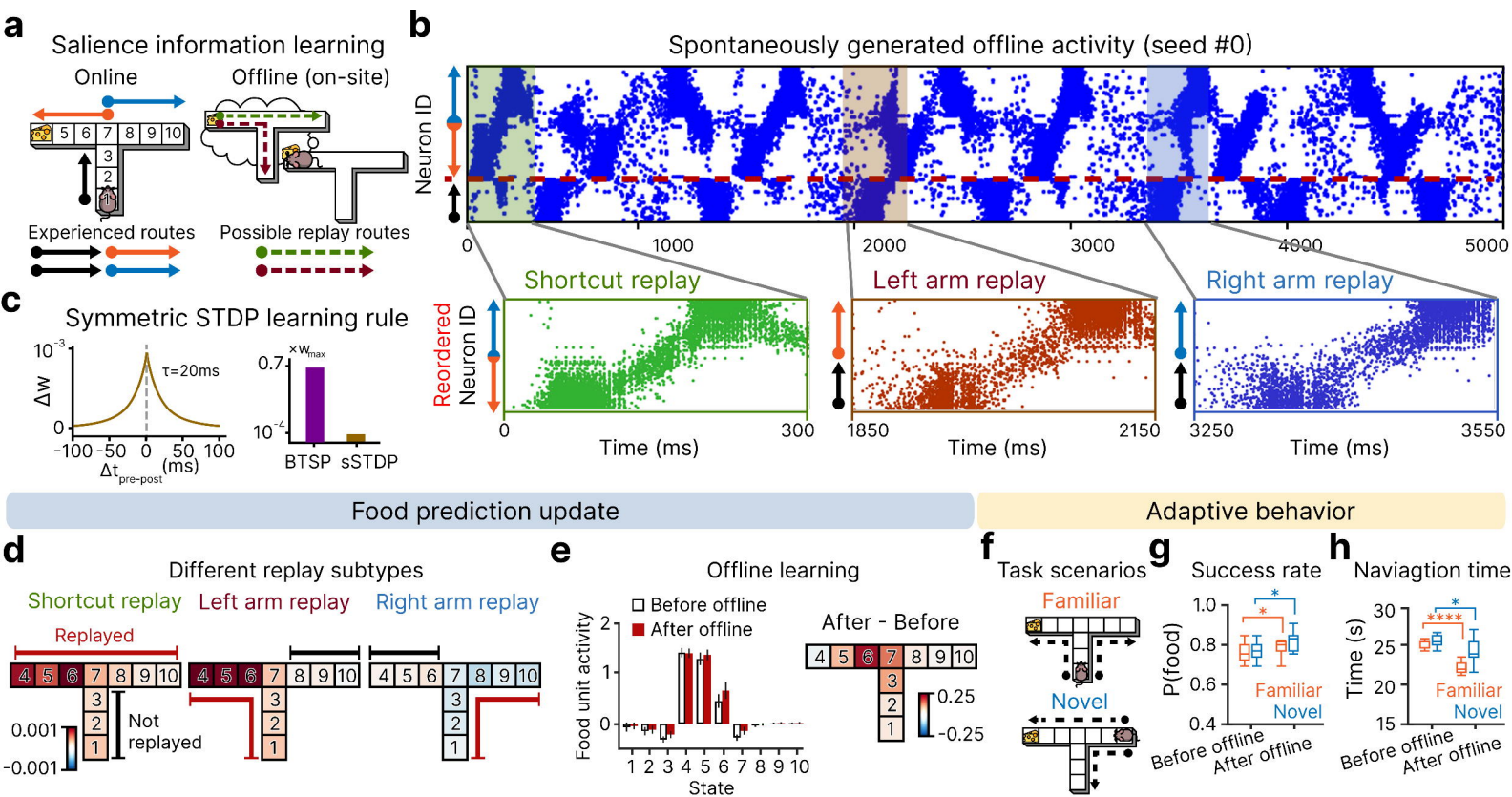
a
Salience information learning
Online
Offline (on-site)
Experienced routes
Possible replay routes
b
Spontaneously generated offline activity (seed #0)
Neuron ID
Shortcut replay
Left arm replay
Right arm replay
Reordered Neuron ID
Time (ms)
c
Symmetric STDP learning rule
τ=20ms
Δw
Δt pre-post (ms)
BTSP
sSTDP
Food prediction update
Adaptive behavior
d
Different replay subtypes
Shortcut replay
Left arm replay
Right arm replay
Replayed
Not replayed
e
Offline learning
Before offline
After offline
Food unit activity
State
After - Before
f
Task scenarios
Familiar
Novel
g
Success rate
P(food)
Before offline
After offline
h
Naviagtion time
Time (s)

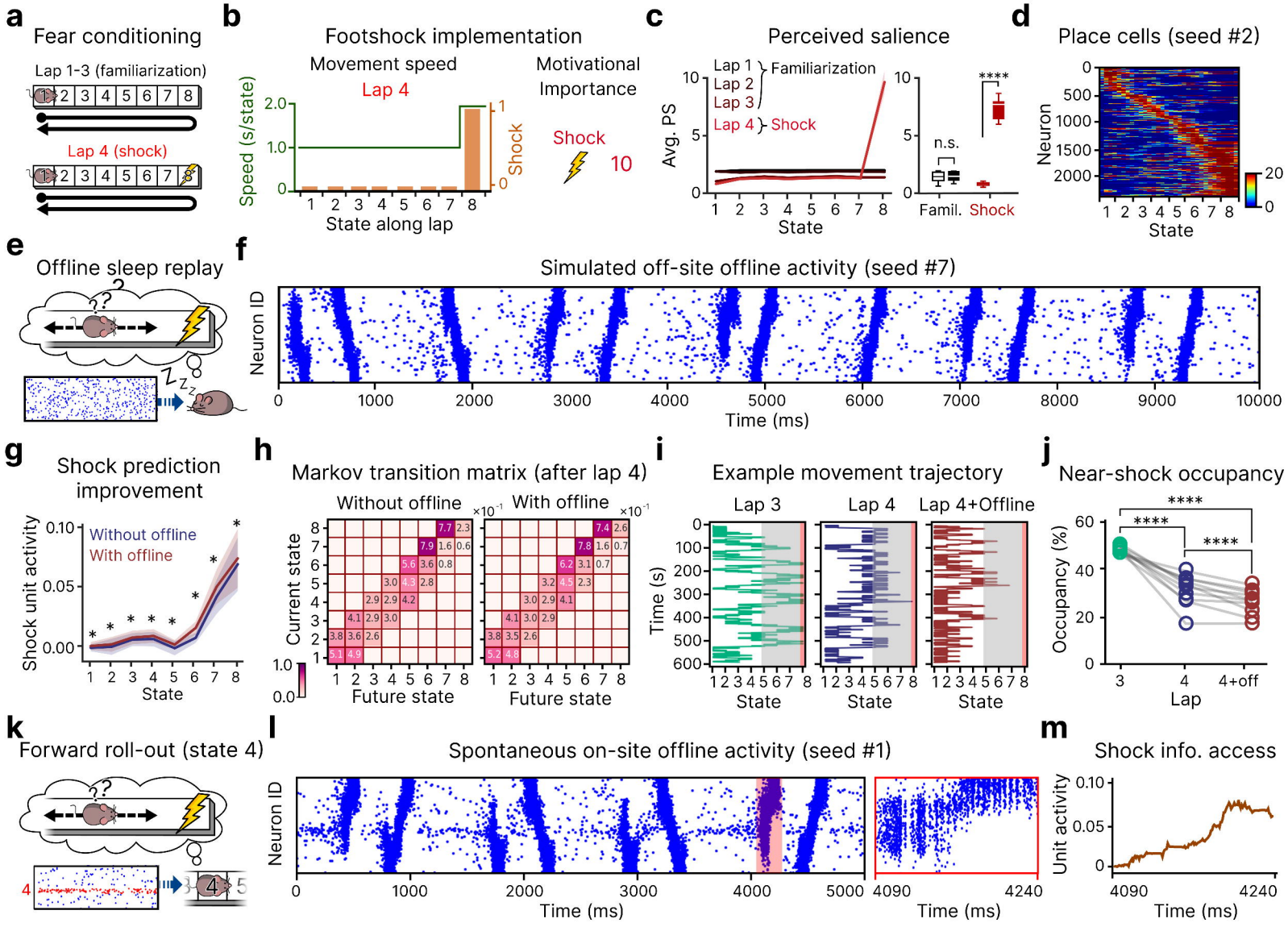
a
Fear conditioning
Lap 1-3 (familiarization)
Lap 4 (shock)
b
Footshock implementation
Movement speed
Lap 4
Speed (s/state)
Shock
State along lap
Motivational Importance
Shock
10
c
Perceived salience
Lap 1
Lap 2
Lap 3
Familiarization
Lap 4
Shock
Avg. PS
State
n.s.
****
Famil.
Shock
d
Place cells (seed #2)
Neuron
State
e
Offline sleep replay
f
Simulated off-site offline activity (seed #7)
Neuron ID
Time (ms)
g
Shock prediction improvement
Without offline
With offline
Shock unit activity
State
h
Markov transition matrix (after lap 4)
Without offline
With offline
Current state
Future state
i
Example movement trajectory
Lap 3
Lap 4
Lap 4+Offline
Time (s)
State
j
Near-shock occupancy
Occupancy (%)
Lap
3
4
4+off
k
Forward roll-out (state 4)
l
Spontaneous on-site offline activity (seed #1)
Neuron ID
Time (ms)
m
Shock info. access
Unit activity
Time (ms)